Published in "Chemical Research in Toxycology 24(9): 1460–1475, 2011"
which should be cited to refer to this work.

Cytotoxicity and Genotoxicity of Size-Fractionated Iron Oxide (Magnetite) in A549 Human Lung Epithelial Cells: Role of ROS, JNK, and NF-κB

Mathias Könczöl,[*,†] Sandra Ebeling,[‡] Ella Goldenberg,[§] Fabian Treude,[‡] Richard Gminski,[†] Reto Gieré,[§] Bernard Grobéty,[∥] Barbara Rothen-Rutishauser,[⊥] Irmgard Merfort,[‡] and Volker Mersch-Sundermann[†]

[†]Department of Environmental Health Sciences, University Medical Center Freiburg, Freiburg, Germany

[‡]Department of Pharmaceutical Biology and Biotechnology, University of Freiburg, Freiburg, Germany

[§]Institute of Geosciences, University of Freiburg, Freiburg, Germany

[∥]Department of Geosciences and FRIMAT, University of Fribourg, Fribourg, Switzerland

[⊥]Departments of Pulmonary Medicine and Clinical Research, Bern University Hospital and University of Bern, Switzerland

ABSTRACT: Airborne particulate matter (PM) of varying size and composition is known to cause health problems in humans. The iron oxide Fe_3O_4 (magnetite) may be a major anthropogenic component in ambient PM and is derived mainly from industrial sources. In the present study, we have investigated the effects of four different size fractions of magnetite on signaling pathways, free radical generation, cytotoxicity, and genotoxicity in human alveolar epithelial-like type-II cells (A549). The magnetite particles used in the exposure experiments were characterized by mineralogical and chemical techniques. Four size fractions were investigated: bulk magnetite (0.2−10 μm), respirable fraction (2−3 μm), alveolar fraction (0.5−1.0 μm), and nanoparticles (20−60 nm). After 24 h of exposure, the A549 cells were investigated by transmission electron microscopy (TEM) to study particle uptake. TEM images showed an incorporation of magnetite particles in A549 cells by endocytosis. Particles were found as agglomerates in cytoplasm-bound vesicles, and few particles were detected in the cytoplasm but none in the nucleus. Increased production of reactive oxygen species (ROS), as determined by the 2′,7′-dichlorfluorescein-diacetate assay (DCFH-DA), as well as genotoxic effects, as measured by the cytokinesis block-micronucleus test and the Comet assay, were observed for all of the studied fractions after 24 h of exposure. Moreover, activation of c-Jun N-terminal kinases (JNK) without increased nuclear factor kappa-B (NF-κB)-binding activity but delayed IκB-degradation was observed. Interestingly, pretreatment of cells with magnetite and subsequent stimulation with the pro-inflammatory cytokine tumor necrosis factor-alpha (TNFα) led to a reduction of NF-κB DNA binding compared to that in stimulation with TNFα alone. Altogether, these experiments suggest that ROS formation may play an important role in the genotoxicity of magnetite in A549 cells but that activation of JNK seems to be ROS-independent.

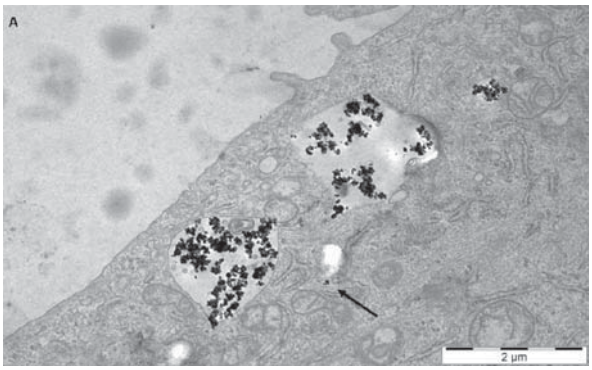

INTRODUCTION

Ambient airborne particulate matter (PM) of varying size and composition is known to cause health problems in humans. These include respiratory and cardiovascular diseases.[1,2] Several epidemiological studies have linked increased mortality or cancer incidence to a higher burden of particles in ambient air. So far, these studies have correlated the health effects to the amounts of PM_{10} (PM with a diameter of <10 μm) and $PM_{2.5}$.[3,4] In recent years, however, the ultrafine particles (UFP, diameter <100 nm) have become the focus of attention because they are predicted to have a higher toxic potential as a result of their high surface/mass ratios.[5] Even though the UFP do not contribute much to the total PM mass, they are dominant in terms of particle numbers, especially in urban areas.[6,7] The UFP are of particular interest to industry because of their special physical and chemical properties, such as increased chemical and biological reactivity, larger active surface area, or enhanced electrical conductivity.[8] There is increasing evidence that UFP have an adverse effect on health,[9,10] but the toxicological knowledge is still poor,[11] and thus, more insight into the interactions between particles and biological structures is urgently needed.

One of the main mechanisms responsible for the adverse health effects induced by atmospheric particles is their ability to generate ROS.[12,13] When produced in abundance, ROS can lead to oxidative stress, i.e., they disturb the balance between oxidative pressure and antioxidant defense, which results in damage to biomembranes. Mitochondria can be targeted by ROS, and the

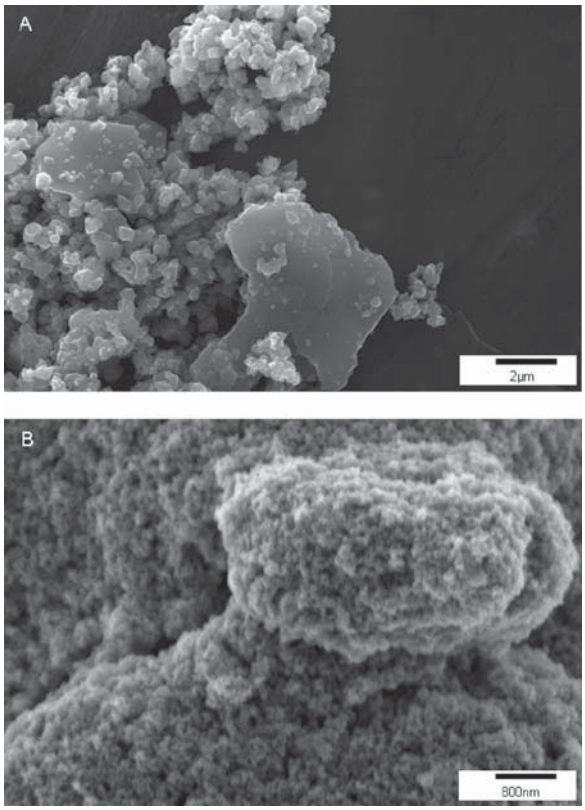

Figure 1. Secondary electron images showing bulk magnetite (A) and MNP (B).

perturbation of the mitochondrial function can lead to apoptosis or DNA damage.[14] Especially metal ions, such as iron ions, derived from PM can catalyze the production of the highly reactive hydroxyl radical, via a series of one-electron reductions.[15]

Magnetite, a spinel-group mineral with the general formula $Fe^{2+}Fe^{3+}{}_2O_4$ (cubic crystal system), is a common natural phase occurring in various rock types, but it is also an important component of many synthetic products, for example, black toner powders.[16] Magnetite particles are also abundant constituents of PM in the urban environment, especially in underground stations,[17,18] along railway lines,[19] or at welding workplaces.[20] Magnetite nanoparticles (MNP) are of special interest in the biological and medical sciences because of their superior biocompatibility compared to that of other magnetic materials, their chemical stability in physiological media, and, moreover, because they can be synthesized easily and economically.[21] MNP are also under investigation as drug carriers.[22] To improve their biocompatibility and to avoid opsonization, MNP are often coated with different polymers, including dextran[23] and polyethylenglycol,[24] but it remains uncertain how well the different coating processes work. Potential gaps in the layer may cause toxic effects in human tissues. Published data on toxicity, especially on cytotoxicity and genotoxicity of nano- and micrometer-sized particles of magnetite, do not give a coherent picture.

No loss of cell viability was determined for bulk and MNP in COS-7,[25] HeLa,[26] and A549 cells.[27] Furthermore, Karlsson et al. found significantly increased DNA damage in A549 cells after 4 h of exposure to 40 $\mu g/cm^2$ of micrometer-sized (<5 μm) magnetite particles.[28] Coated MNP were found to be nontoxic, whereas the bare particles exerted some toxic effects.[11] Cytotoxic effects for noncoated MNP have been found in different cell lines and in *E. coli* but to a varying extent.[29−32] Recently, Zhu and co-workers observed oxidative stress and a decreased mitochondrial membrane potential after the exposure of human umbilical endothelial cells to MNP.[33] Oxidative DNA-lesions (FPG-sites) have been detected for MNP,[27] but no DNA fragmentation was found. Gminski et al. reported genotoxic effects in human lung cells *in vitro* exposed to toner powders containing magnetite, although to a varying extent.[16] After instillation of MNP in mice, an increased expression of pro-inflammatory cytokines and intracellular reduced glutathione was observed.[34] Because of the frequent occurrence of magnetite in the environment, workplace, and in biomedical applications and the lack of consistent data, more systematic investigations on nano- and micrometer-sized magnetite particles are needed to explore their toxic potential.

In this study, we have investigated the cytotoxic and genotoxic potential of different magnetite size fractions and their influence on ROS formation as well as on NF-κB and JNK activation in an A549 cell line (human alveolar epithelial-like type-II cells). The magnetite samples and the reference particles used in this study were characterized by mineralogical methods, including powder X-ray diffraction (XRD) and scanning electron microscopy (SEM). Transmission electron microscopy (TEM) combined with energy-dispersive X-ray spectroscopy (EDX) was used to investigate whether particles were incorporated into the cells and if so into which parts of the cells.

MATERIALS AND METHODS

Chemicals and Reagents. Butylated hydroxyanisole (BHA) (CAS No. 25013-16-5) and ethyl methanesulfonate (EMS) with a purity of >99% (CAS No 62-50-0) were obtained from Alfa Aesar (Karlsruhe, Germany). Stock-solutions were made with DMSO. RPMI 1640 medium was obtained from Invitrogen (Darmstadt, Germany). L-Glutamine, fetal bovine serum (FBS), trypsine/EDTA, and phosphate-buffered saline (PBS) were purchased from PAA (Parsching, Austria). Valinomycin, DCFH-DA, DMSO, neutral red, cytochalasin B, *N*-acetyl-cystein (NAC), H_2O_2 (30%), 4,6-diamidino-2-phenylindole-dihydro-chloride (DAPI), and ethidiumbromide for microscopy were obtained from Sigma-Aldrich (Taufkirchen, Germany).

Particle Source. A bulk magnetite powder (purity ≥97%), consisting of particles with a nominal diameter between 0.2−10 μm, was ordered at Alfa Aesar, Karlsruhe, Germany. This material, termed bulk magnetite (abbreviated as bulk in all diagrams), was used as delivered for all experiments. The bulk magnetite was also used to generate two specific size fractions, namely, the respirable fraction (= RF) (2−3 μm) and the alveolar fraction (= AF) (0.5−1.5 μm). Separation of the bulk magnetite into the RF and AF was performed by connecting a powder dispersion generator (RGB 1000, Palas, Karlsruhe, Germany) to a Berner low-pressure impactor with 5 cascade stages (ISAP B-LPI27/0.05/2.5/10.0, Asendorf, Germany). The fourth type of magnetite used in the experiment, the MNP (purity ≥98%, nominally 20−60 nm), was supplied by Sigma-Aldrich, Taufkirchen, Germany. The particle positive control Min-U-Sil 5 was kindly provided by US Silica, Berkeley Springs, USA.

Particle Characterization. *X-ray Diffraction (XRD).* All magnetite fractions were characterized by powder XRD using a Bruker AXS D8 Advance diffractometer. The magnetite powders were dispersed onto zero-background silicon sample holders and then scanned from 10 to 60°2θ with a step size of 0.01° and a dwell time of 4 s/step using Cu−Kθ radiation. The spectra were compared with the ICPDF database in order to test for the possible presence of impurity phases in the powders.

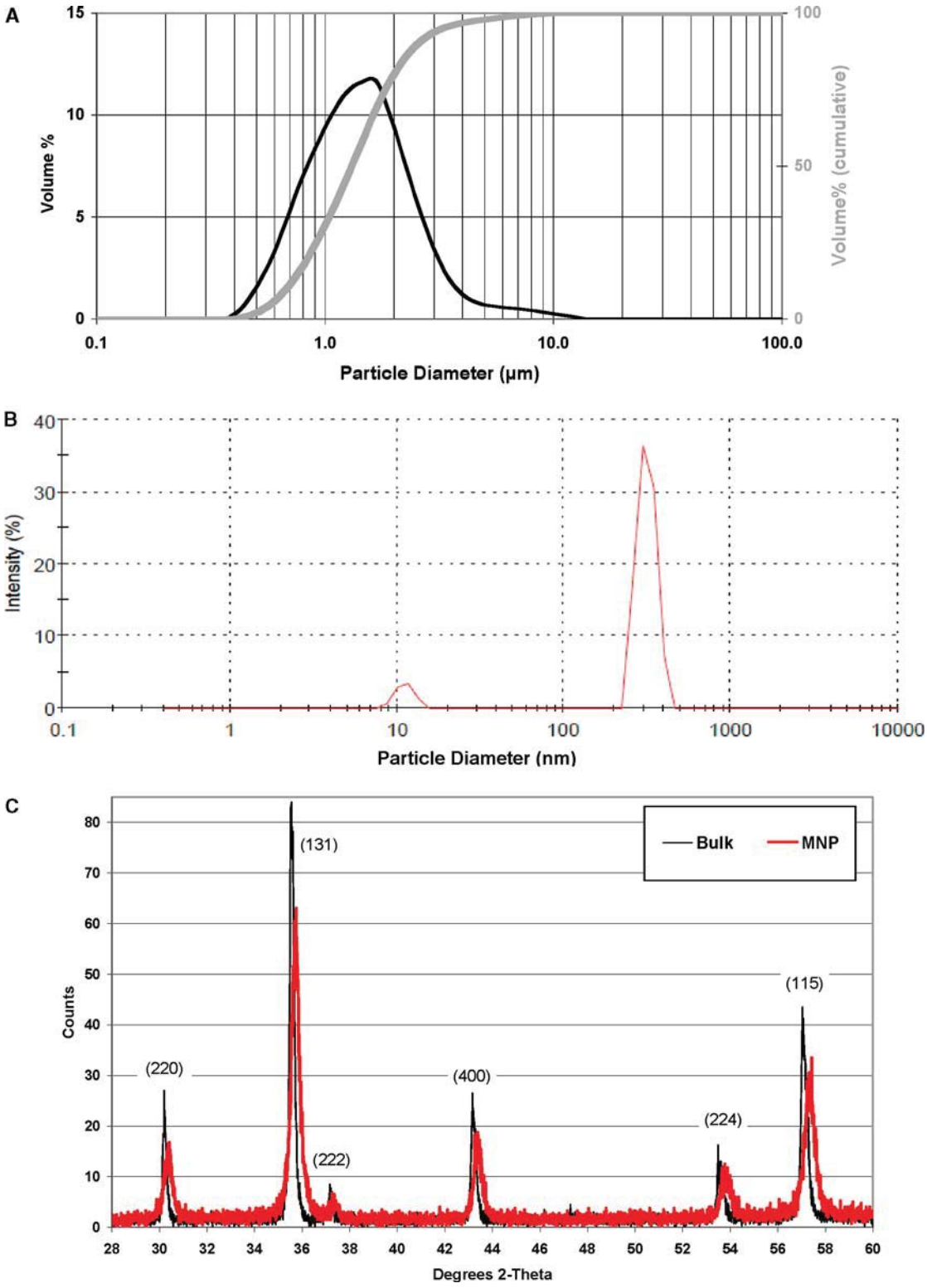

Figure 2. (A) Particle-size distribution of bulk magnetite. The black line shows volume percentage of particles with a specific diameter, revealing that the diameters range from 0.36 to 12.21 μm. The thick gray line shows the cumulative size distribution, documenting that 50% of all particles have diameters <1.31 μm. (B) Particle-size distribution of MNP (100 μg/mL) in RPMI containing 5% FBS derived from PCS measurements. The red line shows the size distribution of MNP with a mean diameter of 311 nm. (C) XRD patterns of bulk magnetite (black line) and MNP (red line) showing the reflections between 28 and 60°2θ. Values in parentheses represent the respective Miller indices for each peak.

Scanning Electron Microscopy (SEM). Particle size and shape were determined using SEM (LEO FE 1525). The magnetite powders were suspended in ethanol and, after 20 min of sonication at 25 °C in an ultrasonic water bath, were pipeted onto an aluminum SEM sample holder and investigated without coating.

Table 1. Chemical Composition of the Bulk Magnetite and the MNP Used in the Toxicological Studies[a]

		bulk magnetite	MNP
element	unit	average (n = 3)	average (n = 3)
Al	ppm	2600 ± 200	3450 ± 50
Cr	ppm	78.3 ± 0.1	82.0 ± 0.1
Fe	wt%	72.0 ± 0.1	71.4 ± 0.5
Mg	ppm	434 ± 2	128 ± 1
Mn	ppm	4720 ± 50	1169 ± 9
Ni	ppm	113 ± 2	6.2 ± 0.2
total[b]	wt%	100.6	99.4
Number of Metal Ions[c] Based on 3 Cations per Formula Unit			
Al^{3+}	mol	0.021	0.030
Cr^{3+}	mol	0.000	0.000
Fe^{3+}	mol	1.978	1.970
Fe^{2+}	mol	0.976	0.994
Mg^{2+}	mol	0.004	0.001
Mn^{2+}	mol	0.020	0.005
Ni^{2+}	mol	0.000	0.000

[a] Concentrations were determined by AAS. [b] Expressed in oxide wt %. [c] Ferrous and ferric iron were calculated from charge balance.

Atomic Absorption Spectroscopy (AAS). To determine the chemical composition of the bulk magnetite and the MNP, the samples were analyzed by AAS after total digestion in a microwave oven (MLS μPREP-A). Digestion took place at 215 °C in an acid mixture consisting of 5 mL of HNO_3 (65%), 1 mL of H_2O_2 (30%), and 2 mL of HF (40%). Iron, Mg, Mn, and Cr were analyzed by flame AAS (Analytik Jena, AAS Vario 6) and Ni and Al by graphite-furnace AAS (Perkin-Elmer 4110 ZL Zeeman).

Size Distribution. To verify the size distribution indicated by the provider, the bulk magnetite powder was analyzed by laser diffraction (Malvern Mastersizer 2000). The sample was dipersed in ethanol (20 min sonication) before analysis. The data were processed with the Mastersizer Microplus software (version 2.19) and by using a density of 5.2 g/cm^3 for magnetite and the refractive indices 2.42 (magnetite) and 1.36 (ethanol). Size distribution of MNP in culture media was analyzed by photon correlation spectroscopy (PCS) (Zetasizer nano-ZS, Malvern Instruments). Samples with 100 μg/mL MNP were dispersed in RPMI containing 5% FBS, followed by 20 min of sonication before analysis. The data was processed with the Zetasizer software (version 6.01).

Preparation of Particle Suspensions. Samples were freshly prepared as particle suspensions prior to each experiment. Particles were suspended in FBS-free culture medium supplemented with 1% L-glutamin and 1% penicillin/streptomycin to a concentration of 5 mg/mL. These suspensions were sonicated for 20 min at 40 °C in an ultrasonic water bath (Sonorex Bandelin, Berlin, Germany) to ensure homogeneous suspensions. Subsequently, the suspensions were diluted in FBS-free culture medium to obtain the required concentrations for each bioassay. Before preparing the Min-U-Sil 5 suspensions, the particles were baked for 16 h at 200 °C to destroy endotoxins that might cause false-positive results in the bioassays, especially with regard to the signaling cascades. Treatment with LPS and Min-U-Sil 5 confirmed that activation of NF-κB was not due to endotoxin contamination. Magnetite was not thermally treated due to the risk of oxidation to hematite (Fe_2O_3) at high temperatures, but the Limulus amebocyte lysate test was performed. No endotoxin contamination was detected.

Cell Culture and Cell Treatment. The human lung adenocarcinoma type-II alveolar epithelial cells A549 were obtained from the DSMZ (Deutsche Sammlung von Mikroorganismen and Zellkulturen GmbH, Braunschweig, Germany). The cells, derived from an individual with alveolar cell carcinoma,[35] have been used extensively to assess type-II cell function because many characteristics of normal type-II cells are retained. The cells were cultured in RPMI culture medium supplemented with 10% FBS, 1% L-glutamin, and 1% penicillin/streptomycin in a humidified incubator at 37 °C with 5 vol % CO_2. For the experiments, cells were trypsinised at 80−90% confluency, seeded into well tissue plates (Greiner, Frickenhausen, Germany), and exposed at 37 °C in a humidified atmosphere containing 5 vol % CO_2.

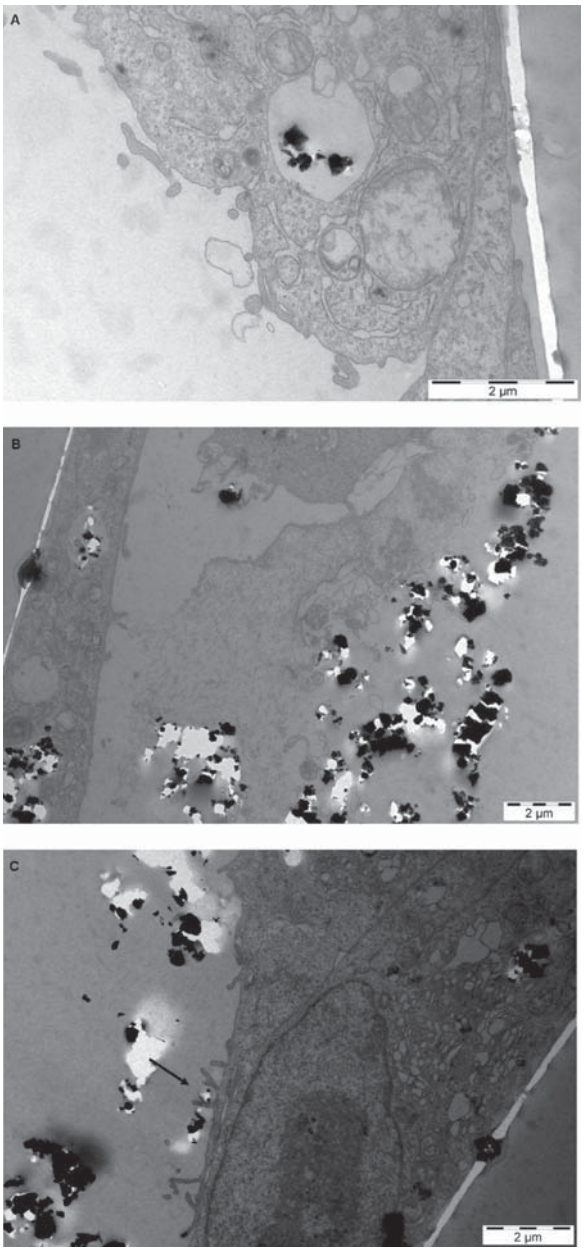

Figure 3. TEM images of A549 cells after 24-h exposure to bulk magnetite (100 μg/cm^2). (A) Magnetite particles in vesicle. (B) Relics of A549 cells next to a large amount of magnetite particles. (C) The arrow points to a spot, where it appears that the particle-uptake mechanism is phagocytosis or micropinocytosis.

Particle Uptake and Localization. Particle uptake of bulk and MNP at concentrations of 10 and 100 μg/cm^2 was investigated by TEM: imaging was performed with Philips Bio CM100 and Philips CM200 equipped with an EDX. For each sample, between 20 and 50 cells were examined. To prepare the samples for the TEM investigation, 1.4 × 10^5

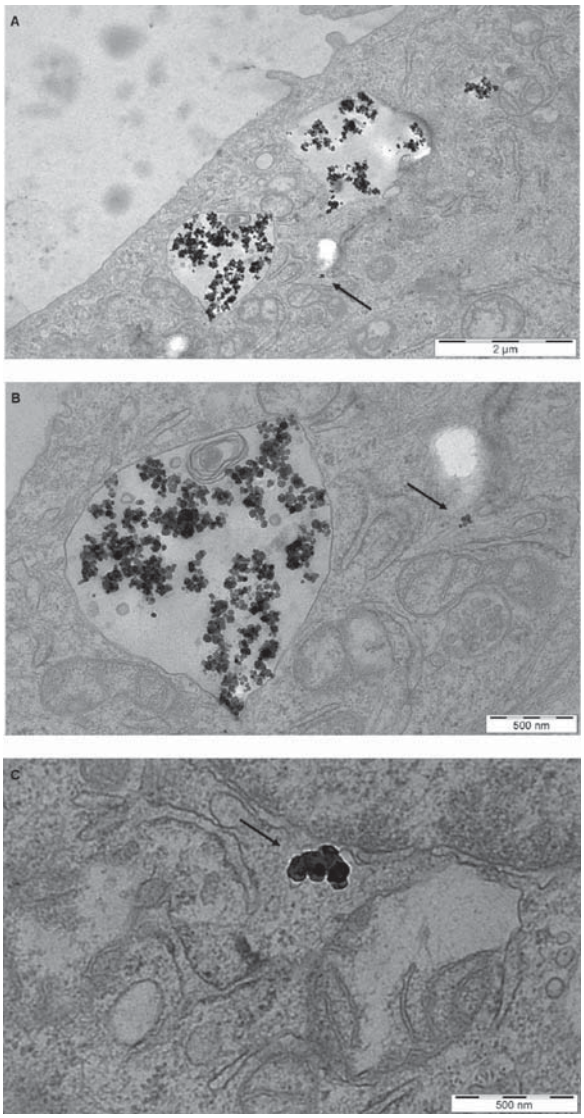

Figure 4. TEM images of A549 cells after 24-h exposure to MNP (10 μg/cm^2). The MNP are enclosed in vesicles but are also within the cytoplasm (arrows).

cells were seeded onto 6-well cell culture inserts (Thincert Greiner, Frickenhausen, Germany) and incubated for 24 h. After 24 h of exposure to particles, cells were washed three times with PBS and subsequently fixed with 2.5% glutaraldehyde (Plano GmbH, Wetzlar, Germany) in 0.03 M potassium phosphate buffer for at least 24 h. Cells were then washed in PBS, postfixed with 1% osmium tetroxide (Simec Services, Aarburg, Switzerland) in sodium carboxylate buffer (Grogg Chemicals, Deisswil, Switzerland), washed with 0.05 mol/L maleate, and stained with 0.5% uranylacetate (Sigma Aldrich, Taufkirchen, Germany) in maleate buffer. After washing the cells in 0.05 mol/L maleate, the cells were dehydrated in a grading series of ethanol followed by acetone, embedded in Epon, and dried in an oven at 60 °C for 4 days.[36] Semi- and ultrathin ($\leq$50 nm) sections were cut parallel to the vertical axis of the embedded cells. Ultrathin sections were put onto copper grids and stained with 1% uranylacetate and lead citrate by using Leica EM stain (Leica Microsystems, Wetzlar, Germany) before the TEM investigation.

Cytotoxicity Assays. Cytotoxicity was determined using two different assays, i.e., the WST-1 assay (Roche diagnostics, Mannheim, Germany), which assesses the metabolic competence of cells, and the neutral red (NR)-uptake assay, which indicates lysosomal activity. Foremost, experiments on the suitability of these cytotoxicity assays were performed to rule out interferences of magnetite particles with assay reagents or detection systems. No adsorption of the dyes to magnetite particles was observed, and light absorption of NR was influenced negligibly for the concentrations tested.

For both assays, 2×10^4 cells were seeded into 96-well plates and grown for 24 h until confluency. The cells were then exposed to 10, 50, 100, 200 μg/cm^2 of particles in RPMI culture medium and additionally with varying contents of FBS in the WST-1 assay, to assess possible interactions between particles and the serum protein, which may mask the toxic effects. After 24 h, the cells were washed twice with PBS.

For the WST-1 assay, cells were then incubated with 100 μL of WST-1 solution (5% WST-1 in RPMI culture medium, 1% L-glutamin, and 1% penicillin/streptomycin) for 1 h at 37 °C. The absorption was measured using a UV−visible spectrophotometer (Tecan infinite M200, Crailsheim, Germany) at 435 nm, with a reference filter at 620 nm. The NR-uptake assay was performed according to the protocol of Repetto et al.[37] with minor modifications. After exposure, cells were incubated with 200 μL of NR-staining solution (4 μg/mL) for 3 h at 37 °C. After washing with PBS, 150 μL of NR-destain solution was added, and the plate was rapidly shaken on a microtiter plate shaker for 20 min to extract the NR from the cells. The absorption was measured at 540 nm, with a reference filter at 645 nm. SiO_2 and DMSO 5% were included as positive controls in each experiment. Each test was performed at least three times independently.

Analysis of Intracellular ROS Production. Oxidative stress was measured by the DCFH-DA assay. DCFH-DA penetrates the cells, where it is hydrolyzed by unspecific esterases and converted into the stable fluorescent product DCF in the presence of oxidative species. 2×10^4 cells were seeded in black 96-well plates and grown in complete culture medium for 24 h until confluency. After washing with PBS, cells were treated with particle suspensions in culture medium for a period ranging from 6 to 24 h. An additional experiment was performed to rule out that iron release from magnetite particles triggers ROS formation. Bulk and MNP suspensions were incubated for 24 h at 37 °C, the supernatant was collected and cells were treated with corresponding concentrations of the supernatant for 24 h. After exposure, cells were rinsed with PBS and incubated with DCFH-DA 10 μmol/L in culture medium without FBS for 30 min. Subsequently, cells were washed twice with PBS, and 100 μL of PBS was added. The green fluorescence (oxidized DCFH-DA), indicating the presence of oxidants, was measured using a spectrophotometer (Tecan infinite M200, Crailsheim, Germany) at an exitation wavelength of 495 nm, with an emission at 528 nm. During the entire procedure with DCFH-DA, the plate was kept out of light to avoid fading of the fluoroprobe. After the fluorescence measurement, the 96-well plate was frozen at −80 °C. To determine the total protein content in each well, the bicinchoninic acid (BCA) assay was used according to the protocol of Olson and Markwell.[38] For cell lysis and extraction of the protein, three freeze−thaw cycles were carried out with the 96-well plate. Fluorescence intensity was expressed in relative fluorescence units (RFU) per μg protein compared to the control cells loaded with DCFH-DA without exposure to particles. Quartz (SiO_2; Min-U-Sil 5) was used as positive control. Each experiment was performed independently in triplicate.

Mitochondrial Membrane Potential (MMP). Measurement of the MMP was carried out with the fluorescent dye JC-1 via flow cytometry as described by Zhao et al.[39]

Single-Cell Gel Electrophoresis (SCGE, Comet) Genotoxicity Assay. The Comet assay was carried out according to the protocols of Singh et al. and Tice et al.[40,41] with minor modifications. Cells (7.5×10^4) were seeded into 12-well plates, incubated for 24 h, and exposed to different concentrations of magnetite for 4 h. The procedure is described in detail by Gminski et al.[16]

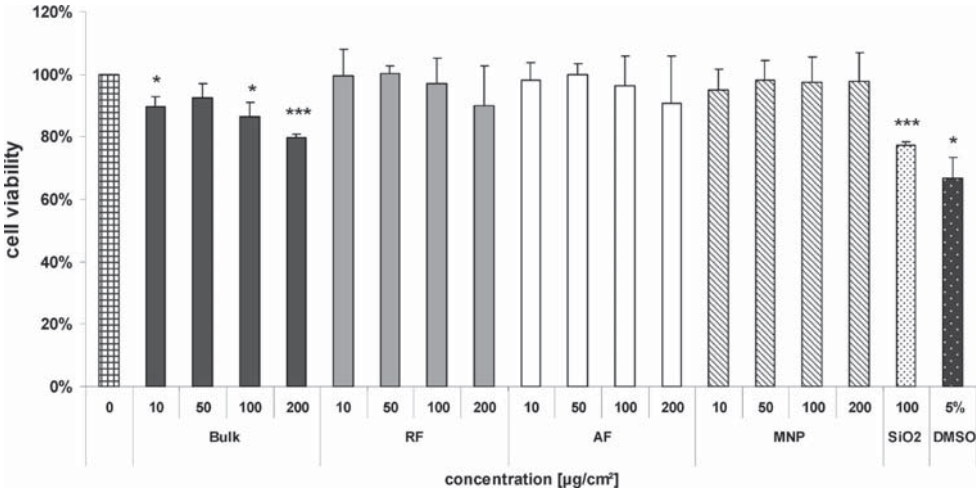

Figure 5. Cell viability as percent viable cells compared to to the untreated control in human lung cells (A549), monitored by the WST assay following 24-h exposure to suspensions containing different size fractions of magnetite. Positive controls: DMSO (5%) and SiO_2 (quartz Min-U-Sil 5, 100 $\mu g/cm^2$). Each bar represents the mean ± SD of at least three independent experiments. $^*p < 0.05$, $^{**}p < 0.01$, and $^{***}p < 0.001$ versus the untreated control (Student's *t* test).

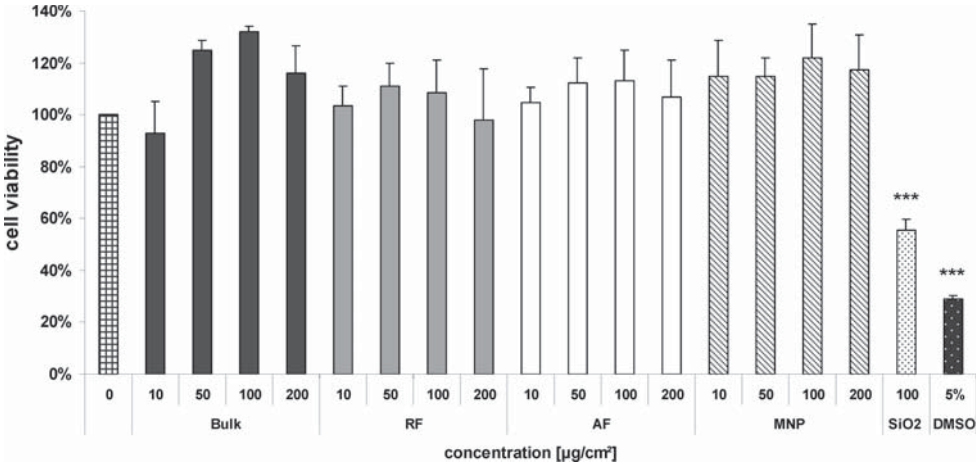

Figure 6. Cell viability as percent viable cells compared to the untreated control in human lung cells (A549), monitored by the NR uptake assay following 24-h exposure to suspensions containing different size fractions of magnetite. Positive controls: DMSO (5%) and SiO_2 (quartz Min-U-Sil 5, 100 $\mu g/cm^2$). Each bar represents the mean ± SD of three independent experiments. $^*p < 0.05$, $^{**}p < 0.01$, and $^{***}p < 0.001$ versus untreated control (Student's *t* test).

To analyze DNA damage in the Comet assay, cells were stained with 60 μL of an ethidiumbromide solution (0.1 μL/mL). Only the slides treated with Min-U-Sil 5 were stained with 50 μL of DAPI (0.2 μg/mL) because of the high self-fluorescence of the Min-U-Sil 5 particles. After staining, the slides were analyzed immediately using a fluorescence microscope DMLS (Leica Microsystems, Wetzlar, Germany) at 400-fold magnification. One hundred randomly chosen cells were analyzed from each slide with an imaging software (Kinetic Imaging 5.5, UK). The extent of DNA migration was evaluated using the parameters olive tail moment (OTM) and tail intensity (TI). OTM is defined as the DNA migration distance multiplied by the relative amount of DNA in the tail of the Comet. TI is defined as the relative amount of DNA in the tail of the comet. Each experiment was performed three times independently.

Cytokinesis Block Micronucleus (CB-MNvit) Genotoxicity Assay. The CB-MNvit assay provides a comprehensive basis for investigating the chromosome-damaging potential *in vitro* because both aneugens and clastogens can be detected. The assay was carried out according to the OECD guideline 487[42] and the protocol of Fenech et al.[43] A suspension of 6×10^4 cells per culture (5 mL) was spread on microscope slides that were kept in chambers of QuadriPERM-dishes so that each single chamber was a separate culture. Cells were exposed to particle suspensions or controls for 24 h. After treatment, cells were cultured for further 24 h in the presence of cytochalasin B (final concentration 3 μg/mL) to block cell division. At the end of the incubation period, cells were washed with PBS twice and treated with 5 mL of trisodium-citrate solution (1.5 wt %) at 37 °C for 6 min, followed by a fixation step with 5 mL of a solution containing 150 mL of ethanol, 50 mL of acetic acid, and 2.5 mL of 37 vol% formaldehyde for 6 min. EMS (a direct-acting clastogen) was used as the positive control. Three independent experiments were performed for each sample.

Microscopic Evaluation and Micronuclei (MN) Scoring. After fixation, the cells were stained with a solution of ethidiumbromide (0.1 μL/mL). Sixty microliters of this solution was placed on the glasslide and covered with a coverslip. The preparations were evaluated using a fluorescence microscope DMLS (Leica Microsystems, Wetzlar, Germany).

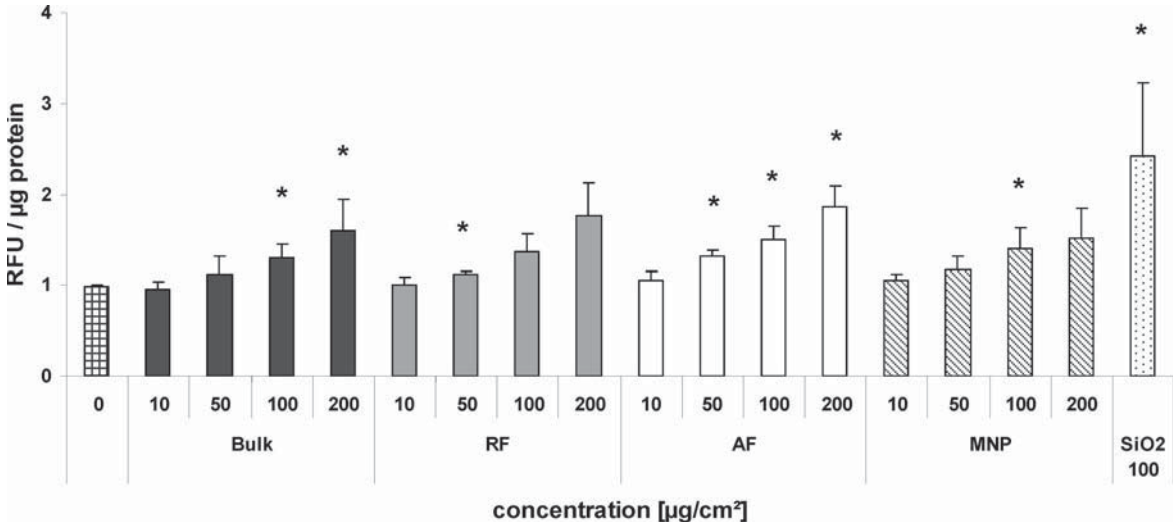

Figure 7. ROS formation in human lung cells (A549), as measured by the DCFH-DA assay after 24-h exposure to different size fractions of magnetite. Results are expressed as relative fluorescent units (RFU) per μg of protein compared to the untreated cells, which were loaded with DCFH-DA without exposure to particles. Positive control: SiO_2 (quartz Min-U-Sil 5, 100 $\mu g/cm^2$). Data represent the mean $\pm$ SD from three independent experiments; $^*p < 0.05$, $^{**}p < 0.01$, and $^{***}p < 0.001$ versus the untreated control (Student's t test).

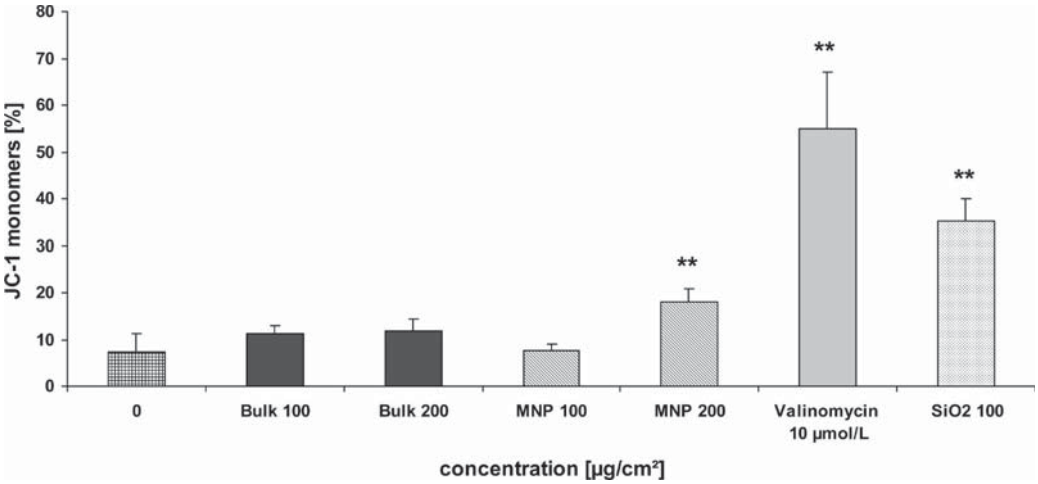

Figure 8. Changes in mitochondrial membrane potential (MMP) induced by bulk magnetite and MNP in human lung cells (A549) upon 24-h treatment. Cells were stained with 2 μg/L JC-1 for 0.5 h. Appropriate gates were made to define JC-1 aggregates and JC-1 monomers. MMP is expressed as the percentage of JC-1 monomers. Positive controls: SiO_2 (quartz Min-U-Sil 5, 100 $\mu g/cm^2$) and Valinomycin (10 μmol/L). Data represent mean $\pm$ SD from three independent experiments; $^*p < 0.05$, $^{**}p < 0.01$, $^{***}p < 0.001$ versus untreated control (Students t test).

All slides were coded before scoring. The binucleated cells (BNC) were selected according to the criteria described in refs 44 and 45. Apoptotic and necrotic cells were included in the total cell number, but micronuclei were not scored in these cells. For each sample, the number of micronuclei (MN) in 1000 BNC was determined, and the MN/1000 BNC ratio was calculated. To rule out cytotoxic effects, the cytochalasin block proliferation index (CBPI) of each sample was evaluated according to Surralles et al.[46] by assessing 500 cells. The CBPI indicates the number of cell cycles per cell during the period of exposure to cytochalasin B and is calculated as follows:

$$\mathrm{CBPI} = \frac{(\text{no. of mononucleated cells}) + (2 \times \text{no. of BNC}) + (3 \times \text{no. of multinucleated cells})}{\text{total number of cells counted}}$$

Electrophoretic Mobility Shift Assay (EMSA). The influence of the particles on NF-κB DNA-binding was determined by the electrophoretic mobility shift assay. Cells (5×10^5) were seeded into 6-well plates and grown to 60−70% confluence. Twenty-four hours before particle treatment, the medium was changed to starvation medium (0% FCS). After incubation with different particle concentrations and time durations,

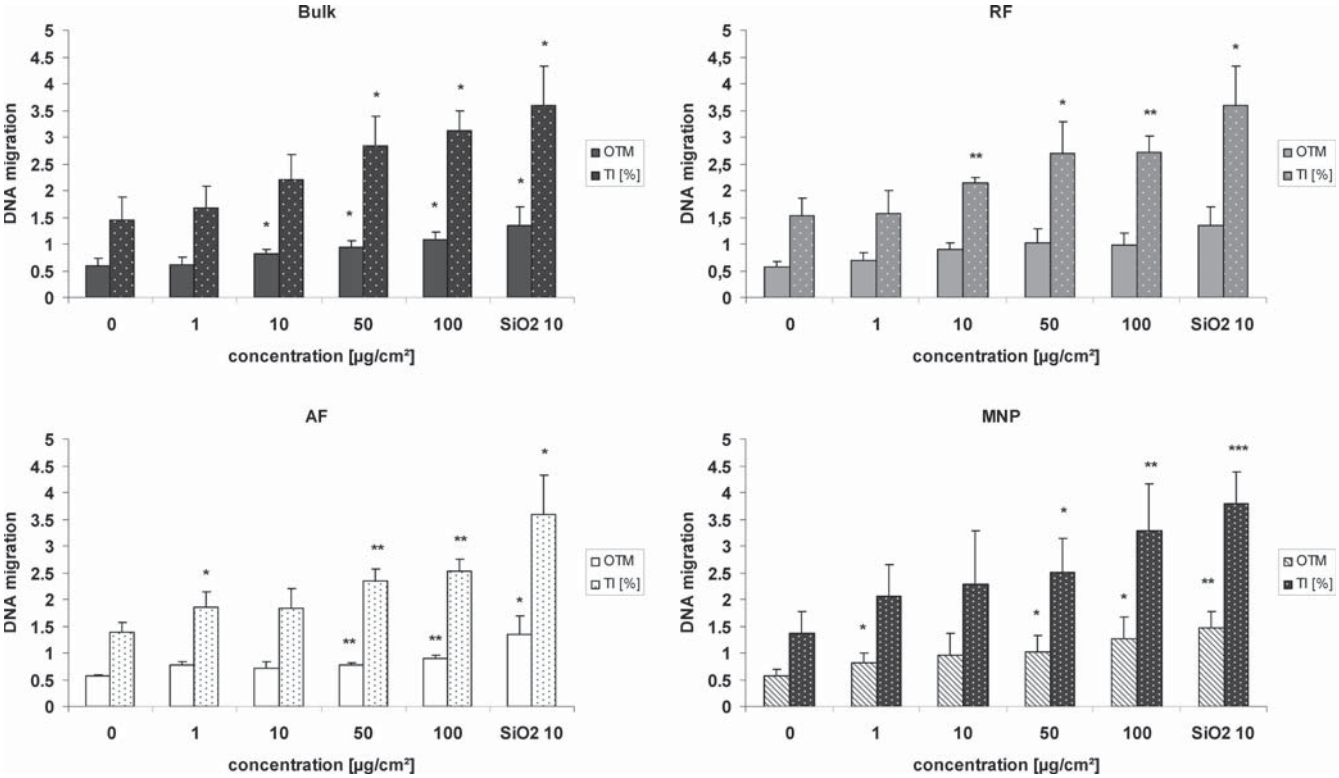

Figure 9. DNA migration (olive tail moment, OTM; tail intensity, TI, in %), assessed by the Comet assay, in human lung cells (A549) after 4-h exposure to suspensions containing different size fractions of magnetite. Positive control: SiO_2 (quartz Min-U-Sil 5, 10 $\mu g/cm^2$). Data are the mean ± SD of three independent experiments. $^*p < 0.05$, $^{**}p < 0.01$, and $^{***}p < 0.001$ versus untreated control (Student's t test).

nuclear extracts were obtained as described previously by Schreiber et al.[47] Additionally, cells were stimulated for 30 min with human TNFα (4 ng/mL, PeproTech, Hamburg, Germany) alone (as positive control) and after particle pretreatment with different concentrations and times (100−400 $\mu g/cm^2$, 1 to 6 h).

The Bradford protein assay (BioRad, München, Germany) was used to determine the concentration of the nuclear protein extract. Five micrograms of the protein extract were added to a reaction mixture containing 20 μg of bovine serum albumin, 2 μg of poly(dI-dC) (Roche Diagnostics, Mannheim, Germany), 2 μL of buffer D+ (20 mM Hepes/KOH at pH 7.9, 20% glycerol, 100 mM KCl, 0.5 mM EDTA, 0.25% Nonidet P-40, 2 mM DTT, and 0.1% phenylmethylsulfonyl fluoride), 4 μL of buffer F (20% Ficoll 400, 100 mM Hepes/KOH at pH 7.0, 300 mM KCl, 10 mM DTT, and 0.1% phenylmethylsulfonyl fluoride), and 25 ng of [γ^{33}P]-labeled NF-κB oligonucleotide to a final volume of 21 μL. The NF-κB oligonucleotide (5′-AGT TGA GGG GAC TTT CCC AGG C-3′ and 3′-TCA ACT CCC CTG AAA GGG TCC G-5′, Promega, Mannheim, Germany) was labeled using [γ^{33}P]ATP (3000 Ci/mmol, Hartmann Analytic, Braunschweig, Germany) and a T4 polynucleotide kinase (New England Biolabs, Hilden, Germany). For competition experiments, the reaction mixture contained a 100-fold excess of the nonradioactive labeled oligonucleotide. Samples and reaction mixture were incubated at room temperature for 25 min and resolved through a nondenaturating 6% polyacrylamide gel. The gel was transferred to a Whatman 3MM paper and dried under vacuum at 80 °C for 60 min. After drying, the gel was exposed to a PhosphoImager BAS film (Fujifilm, Düsseldorf, Germany) for 24 h. Detection was performed by PhosphoImager. The resulting images are shown together with the quantified [γ^{33}P]-stimulated luminescence (PSL) units of each specific shift.

Phospho-JNK, IκBα, and Heat Shock Protein 70 (Hsp70) Western Blot. The influence of magnetite on JNK, IκBα, and Hsp70 was determined by Western blot analysis. Cells (0.6×10^6) were seeded into 6-well plates (3 wells per sample) and grown to 60−70% confluence. The medium was changed to starvation medium (0% FCS) 24 h before stimulation. For pJNK Western blots, cells were treated with 100 $\mu g/cm^2$ MNP for 10 to 36 h. A combination of actinomycin D (333 nmol/L) and TNFα (4 ng/mL) served as a positive control. To determine the role of ROS in JNK-activation, BHA (200 μmol/L), or NAC (1−2 mmol/L) were added 30 min before stimulation. For IκBα Western blots, cells were treated with 200 $\mu g/cm^2$ MNP or 1 mmol/L sodium arsenite for 2 h, returned to starvation medium for 1 h, and stimulated with TNFα (4 ng/mL) for 10 to 60 min. For Hsp70 Western blots, cells were treated with 200−400 $\mu g/cm^2$ MNP or 1 mmol/L sodium arsenite for 2 h and returned to starvation medium for 4 h. For the preparation of total extracts, cells were washed with PBS and centrifuged (148g, 4 °C, 5 min), and 126 μL of Triton X lysis buffer (136 mmol/L NaCl, 20 mmol/L Tris/HCl at pH 7.4, 10% glycerol, 2 mmol/L EDTA, 50 mmol/L β-glycerophosphate, 20 mmol/L Na-pyrophosphate, 10 mmol/L NaF, 4 mmol/L benzamidine, 1 mmol/L Na-vanadate, and 1% Triton X 100) supplemented with protease inhibitors (0.2 mmol/L pefablock, 5 μg/mL aprotinin, and 5 μg/mL leupeptin) and phosphatase inhibitors (10 μL/mL PhosStop (Roche Diagnostics, Mannheim, Germany)) were added. Cell lysis was performed by shaking for 20 min at 4 °C. The supernatant was collected after centrifugation (20200g, 4 °C, 10 min).

To analyze the protein level in the cell lysate, samples containing 40−100 μg of protein were separated by SDS−PAGE (12% gel) and transferred to a 0.4 μm pore size PVDF membrane (Roche Diagnostics, Mannheim, Germany). Antigen detection was done using antibodies against p-JNK, JNK, and IκBα (Cell Signaling, Boston, USA, 1:1000, 5%

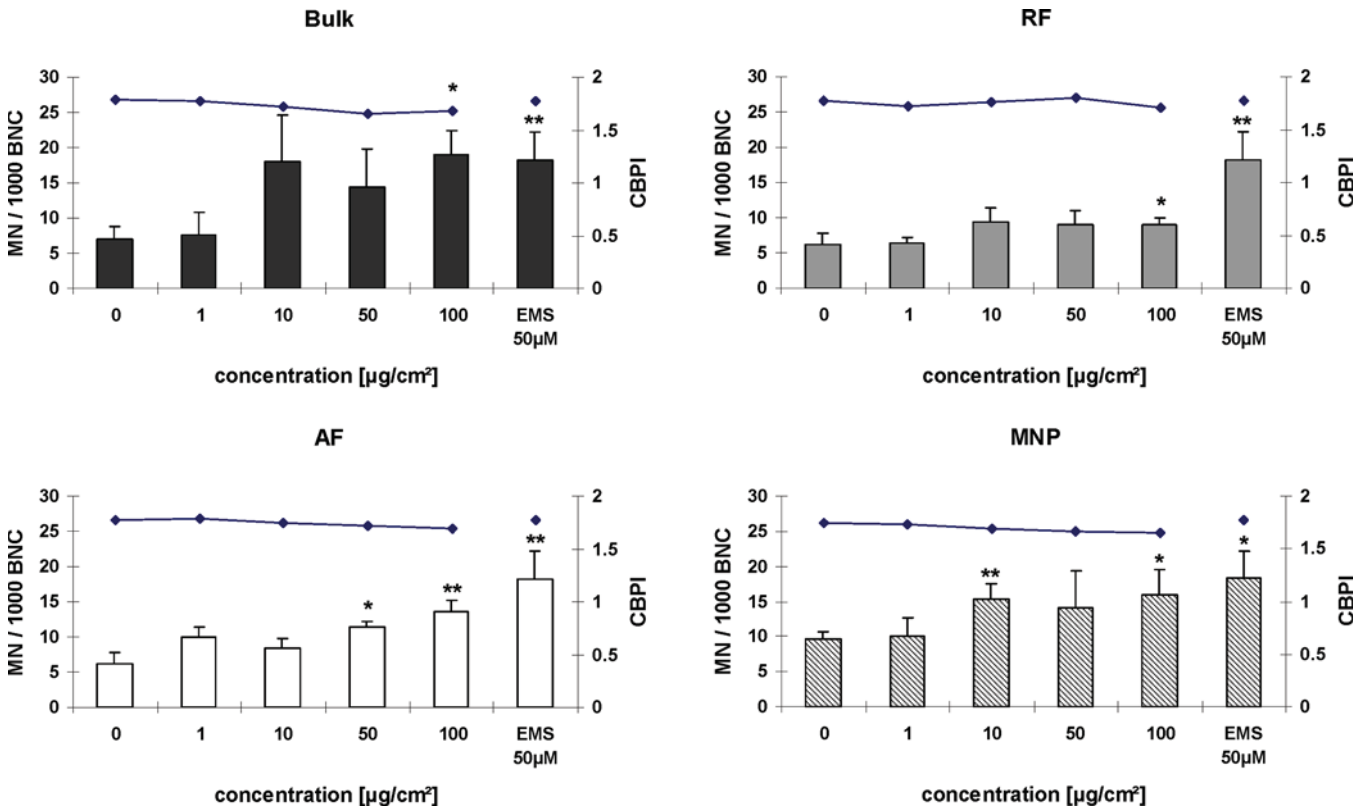

Figure 10. Cytokinesis block proliferation index (CBPI) (diamonds) and micronuclei induction (bars) in human lung cells (A549) upon 24-h treatment with suspensions containing different size fractions of magnetite. Positive control: EMS (50 μmol/L). Data represent the mean ± SD from four independent experiments; $^{*}p < 0.05$, $^{**}p < 0.01$, and $^{***}p < 0.001$ versus the untreated control (Student's t test); MN, micronuclei; BNC, binucleated cells.

BSA in TBST (TBS buffer containing 0.1% Tween 20)), Hsp70 (Enzo Life Sciences, Lörrach, Germany, 1:1000, 5% BSA in TBST), β-actin (MP Biomedicals, Illkirch, France, 1:10000, 1% BSA in TBST), an appropriate horseradish peroxidase-labeled secondary antibody, and an ECL plus chemiluminescence detection reagent (GE Healthcare, Munich, Germany and P.J.K., Kleinblittersdorf, Germany). Chemiluminescent images were taken using the LumiImager and the LumiAnalyst Software (Roche Diagnostics, Mannheim, Germany).

Statistical Analysis. Statistical analysis was performed using MsExcel 2000. All data presented are given as the mean ± standard deviation (SD) of at least three independent experiments. Data shown for the Comet assay are the mean OTM ± SD and tail intensity [%] ± SD. For the CB-MNvit test, all data are expressed as the mean ± SD of MN/1000 BNC. Differences among treatments compared to those of solvent controls were evaluated by the unpaired two-tailed Student's t test with unequal variance. A difference was considered significant at $p < 0.05$.

RESULTS

Particle Characterization. SEM imaging revealed that the bulk magnetite powder consists of particles ranging in size from 0.2 to 10 μm and that it contains euhedral crystals (octahedra), sharp plates, and irregularly broken to slightly rounded particles (Figure.1A). The SEM observation related to size has been confirmed by laser diffraction analysis (Figure 2A). The laser diffraction data reveal that the particle diameters range from 0.36 to 12.21 μm, with a distinct maximum between 1.43 and 1.67 μm (black line in Figure 2A). The data further show that 50% of all particles have diameters <1.31 μm (thick gray line). The PCS measurement shows that MNP dispersed in RPMI containing 5% FCS are mainly present as aggregates. For a concentration of 100 μg/mL, a size distribution with a mean diameter of 311 nm and a polydispersity index (PDI) of 0.481 was obtained (Figure 2B). Another peak can be seen at 10 nm, derived from the serum components of the culture media. From the laser diffraction data, we calculated a specific surface area of 0.9929 m^2/g for the bulk magnetite powder. Such detailed data are not available for MNP because the particles have dimensions that lie outside the reliable size range of our laser diffraction instrument. The SEM investigations, however, show that the MNP are 20−60 nm across and rounded to slightly elongated (Figure 1B).

The XRD patterns of both bulk magnetite and MNP confirmed the mineralogical identity of samples and documented that no other phase was present. The XRD reflections for the MNP are broader and exhibit lower intensity compared to those of bulk magnetite (Figure 2C), consistent with a smaller crystallite size of the MNP material. The XRD peaks for MNP are also shifted to slightly higher 2θ values, which is especially very visible for the reflection corresponding to the planes with the (115) Miller index (Figure 2C). These peak shifts indicate that the two materials are chemically different. This conclusion is supported by the AAS data (Table 1): the differences in chemical composition of the two materials are significant for the analyzed minor constituents but not for Fe (Table 1). Compared to MNP, the bulk magnetite sample is considerably richer in Mg, Mn, and Ni but poorer in Al.

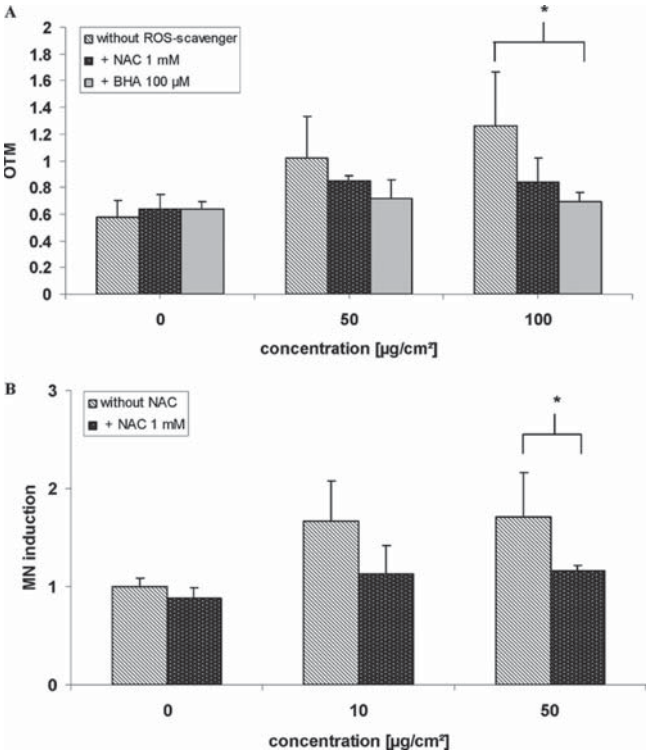

Figure 11. DNA migration (A) and micronuclei induction (B) in human lung cells (A549) after 4-h (Comet assay) or 24-h (CB-MNvit) exposure to suspensions containing different concentrations of MNP with or without simultaneous incubation with the ROS-scavengers NAC and BHA. Data are the mean ± SD of three independent experiments. $^{*}p < 0.05$, $^{**}p < 0.01$, and $^{***}p < 0.001$ versus the untreated control (Student's *t* test).

Particle Uptake. The A549 cells, which were exposed to the bulk magnetite powder, accommodated particles with diameters <1 μm. The TEM investigations revealed that these particles were incorporated into membrane-bound vesicles, mainly as small aggregates that consist of 2 to 10 particles (Figure 3A). Some cells seem to have been destroyed by particle overload (Figure 3B).

In cells exposed to MNP (Figure 4), membrane-bound vesicles of varying sizes contained large aggregates (100−200 μm in diameter) consisting of several tens to hundreds of MNP. A few clusters consisting of less than 10 particles were incorporated directly into the cytoplasm. Screening of approximately 100 cells revealed only one MNP located inside a cell nucleus.

Cytotoxicity. The magnetite samples were found to be only slightly cytotoxic, and cytotoxicity does not depend on the amount of FBS in the culture medium. With an FBS content of 5%, only the samples exposed to the highest concentration of the bulk powder (200 $\mu g/cm^2$) showed a significant decrease in viable cells, as measured by the WST-1 assay (80 ± 1%; $p < 0.001$) (Figure 5), whereas no further significant reduction of viability was found when the FBS content of the culture medium was decreased (data not shown). No cytotoxicity was observed for the NR-uptake assay after 24-h particle exposure (Figure 6).

ROS Production. After 6 h of exposure to magnetite fractions, ROS production increased only slightly as a function of concentration (data not shown). However, after 24 h of exposure, a significant concentration-dependent ROS production was observed for all fractions ($p < 0.05$) (Figure 7), but only slight differences between the different particle sizes were observed. No increased ROS formation was observed after 24 h of exposure to the supernatant of media incubated with bulk or MNP for 24 h (data not shown). The samples exposed to the bulk powder showed a significant increase at 100 $\mu g/cm^2$ and 200 $\mu g/cm^2$ (1.29- and 1.59-fold, respectively; $p < 0.05$), whereas for the RF, a significant increase was found only at a concentration of 50 $\mu g/cm^2$ (1.11-fold; $p < 0.05$). The AF exhibited the largest concentration-dependent increase in ROS production, with a significant 1.86-fold at 200 $\mu g/cm^2$ ($p < 0.05$). MNP induced significantly increased ROS formation at a concentration of 100 $\mu g/cm^2$ (1.4-fold; $p < 0.05$).

Mitochondrial Membrane Potential (MMP). After 24 h of exposure to the different magnetite fractions, the amount of JC-1 monomers, as a marker of depolarization of the mitochondrial membrane, increased in a concentration-dependent manner for bulk magnetite and MNP (Figure 8). However, only MNP showed a significant increase in JC-1 monomers at a concentration of 200 $\mu g/cm^2$ (17.92 ± 3.02%; $p < 0.05$) compared to that of the untreated control (7.32 ± 4.02%).

Induction of DNA Migration. All magnetite fractions induced DNA damage in a concentration-dependent manner after 4 h (Figure 9). Significantly increased DNA migration, as measured by the parameters OTM and TI, was observed for all fractions at concentrations of 50 $\mu g/cm^2$ ($p < 0.05$). Bulk and MNP show the highest levels of DNA migration (ranging from 1.7- to 2.6-fold). The effects of all magnetite fractions were less pronounced than those induced by the positive control SiO_2 (Min-U-Sil 5, 10 $\mu g/cm^2$). The DNA-damaging effect was reduced by simultaneous addition of 1 mmol/L NAC to the A549 cells or by pretreatment with 100 μmol/L BHA, both ROS-scavengers, at two different concentrations of MNP (Figure 11A). The inhibitory effect was higher for the cells pretreated with BHA (65−83%) than that for cells incubated with NAC (39−61%).

Induction of Micronuclei Formation. The level of induced MN in A549 cells after 24 h of exposure to the different magnetite fractions is shown in Figure 10. MN formation in BNC resulting from the treatment of cells only with supplemented culture medium was 6 to10 MN/1000 BNC. The positive control (EMS, 50 μmol/L) showed an incidence of MN formation of 18.25 ± 3.9 MN/1000 BNC (Figure 10). The highest effects were observed for cells exposed to the bulk powder, AF and MNP. In the case of bulk magnetite, the formation of MN was concentration-dependent, reaching a maximum of 19 ± 3.5 MN/1000 BNC at 100 $\mu g/cm$ ($p < 0.05$). AF showed an increased MN formation at 50 $\mu g/cm^2$ (11.5 ± 0.7 MN/1000 BNC; $p < 0.05$), increasing further to 13.7 ± 1.5 MN/1000 BNC at 100 $\mu g/cm^2$ ($p < 0.01$). For MNP, significantly enhanced MN induction was already observed at 10 $\mu g/cm^2$ (15.3 ± 2.2 MN/1000 BNC; $p < 0.01$), reaching a maximum of 16 ± 3.5 MN/1000 BNC at 100 $\mu g/cm^2$ ($p < 0.05$). The RF showed the lowest MN formation with a maximum of 9.3 ± 2.0 MN/1000 BNC. CBPI revealed no inhibition of cell proliferation in any of the samples analyzed (see Figure 10, diamonds). Simultaneous addition of the ROS scavenger NAC (1 mmol/L) together with two different concentrations of MNP to A549 cells decreased MN formation almost to the level of that of the untreated control (Figure 11B). The inhibitory effect reached between 77.6 and 80.8% for the two concentrations tested.

Activation of NF-κB. The bulk and the MNP fractions were studied for their effect on NF-κB DNA binding. After short exposure times (1−6 h), samples exposed neither to bulk magnetite

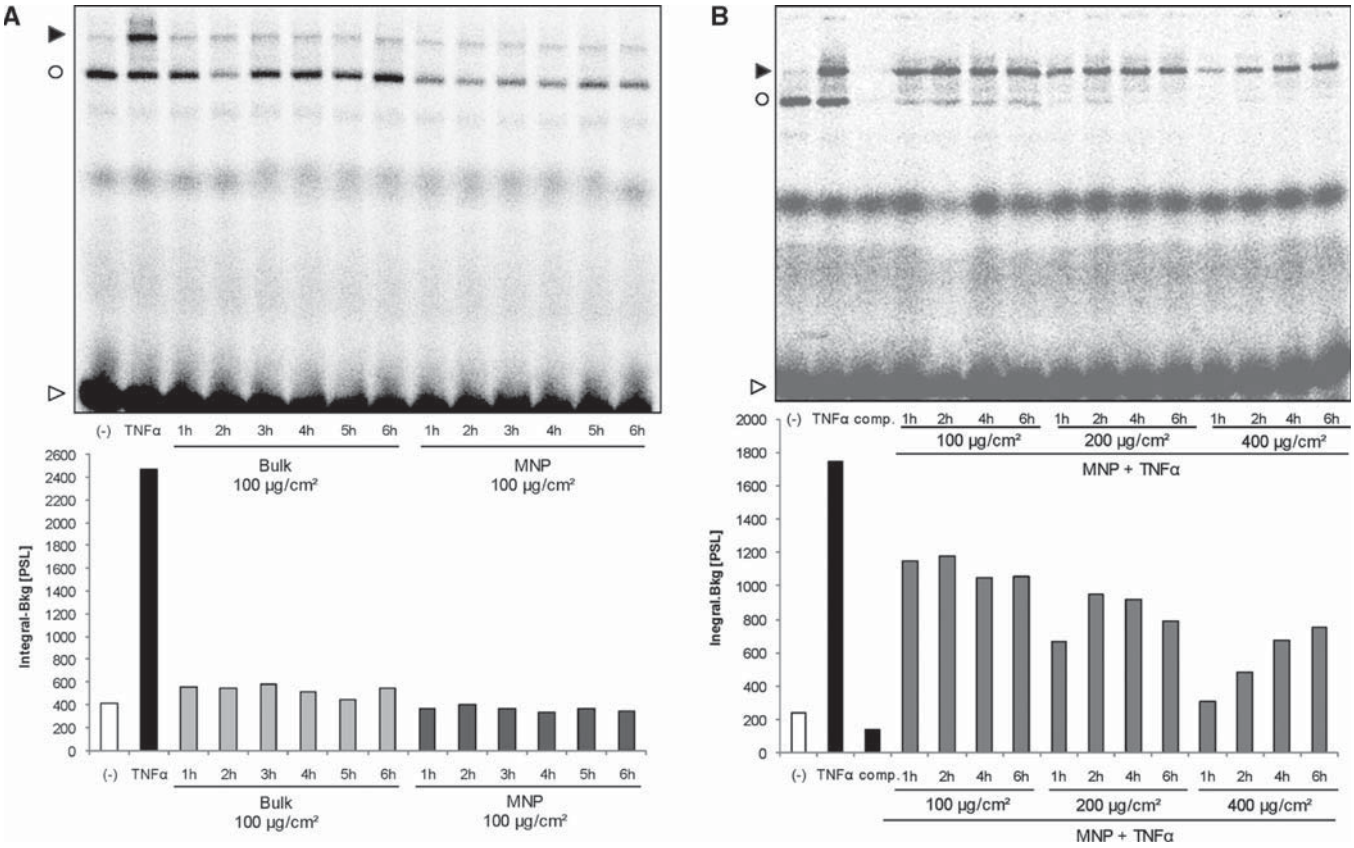

Figure 12. (A) Effect on NF-κB DNA binding after the exposure of A549 to bulk magnetite and MNP. Lane 1 shows unstimulated control cells; lane 2, cells stimulated with TNFα (4 ng/mL, 30 min) as the positive control; in the other lanes cells were treated with bulk magnetite and MNP (100 μg/cm^2) for 1 to 6 h. (B) Effect on TNFα-induced NF-κB activation after pretreatment with MNP. Lane 1 shows unstimulated control cells, lane 2 cells stimulated with TNFα (4 ng/mL, 30 min); comp., competition assay; incubation of the radioactive labeled oligonucleotide complex with unlabeled oligonucleotide; in the other lanes, cells were pretreated with different concentrations of MNP (100, 200, and 400 μg/cm^2) and subsequently stimulated with TNFα (4 ng/mL, 30 min). Equal amounts of protein from cell extracts were analyzed for NF-κB activity by EMSA. A filled arrowhead indicates the position of NF-κB DNA complexes. The open circle denotes a nonspecific activity binding to the probe, and the open arrowhead shows unbound oligonucleotide. One representative EMSA is shown.

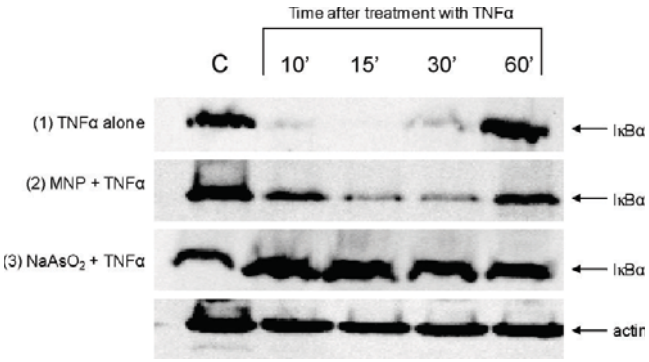

Figure 13. Reduced IκBα degradation by TNFα after MNP stimulation. Western blot analysis of IκBα after 2 h of treatment of MNP (200 μg/cm^2) or the positive control sodium arsenite (1 mmol/L) and stimulation with TNFα (4 ng/mL) for the indicated durations. One representative Western blot is shown. C means untreated control cells. Actin normalization of blot 2 is shown; those of blots 1 and 3 give the same results and are not shown.

(100 μg/cm^2) nor to MNP (100 μg/cm^2) showed an increased NF-κB DNA binding activity (Figure 12A). The same results were obtained for concentrations up to 400 μg/cm^2 and after long-time stimulation (12, 24, and 48 h) at concentrations of 100 and 200 μg/cm^2 (data not shown). Treatment with TNFα (4 ng/mL, 30 min) resulted in a strong NF-κB activation. Additional experiments were performed to analyze the effect of MNP on TNFα-induced NF-κB activation (Figure 12B). Interestingly, particle pretreatment and subsequent stimulation with TNFα for 30 min led to a decrease in NF-κB activation compared to that with the treatment with TNFα alone. This effect could be observed for each exposure time and is more pronounced at higher concentrations. The specificity of the NF-κB DNA binding was determined by using a 100-fold excess of nonradioactive NF-κB oligonucleotide (Figure 12B, comp.).

In unstimulated cells, NF-κB is retained in the cytosol by IκBα. Stimulation with TNFα leads to degradation of IκBα and subsequent translocation of NF-κB to the nucleus where it exerts its transcriptional function. To study whether the observed decrease of TNFα-induced NF-κB activation by MNP can be explained by influencing IκBα degradation, further experiments were performed. In cells treated only with TNFα, a time-dependent degradation of IκBα occurred which started 10 min after TNFα stimulation and returned to control level after 60 min through newly synthesized IκBα, which is a target gene from NF-κB (see Figure 13, (1)). Treatment of the cells with

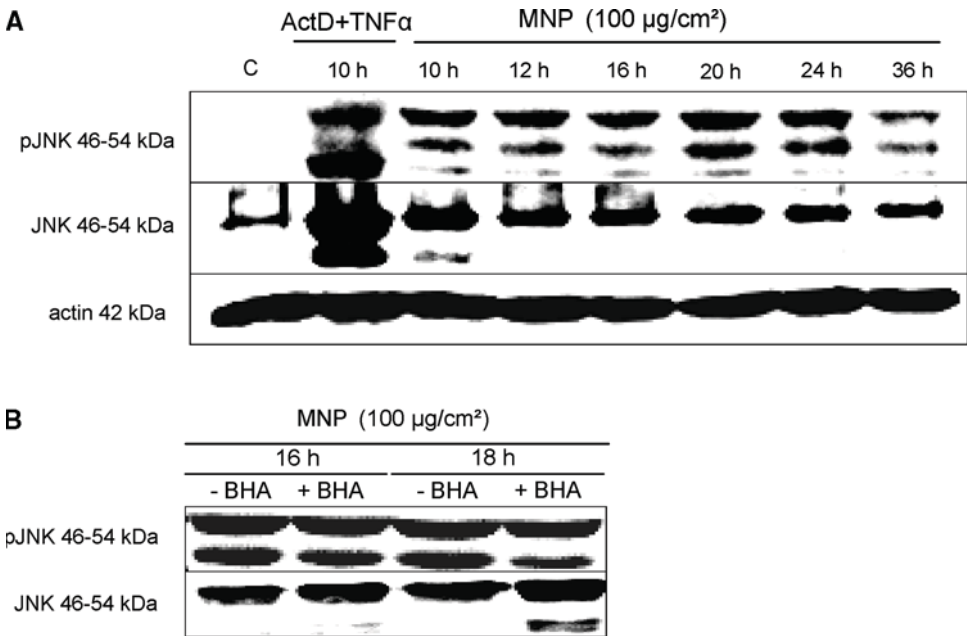

Figure 14. Activation of c-Jun N-terminal kinase (JNK) by MNP. Western blot analysis of phospho-JNK (p-JNK) after treatment with MNP (100 μg/cm^2) for the indicated times. A combination of actinomycin D (ActD, 333 nmol/L) and TNFα (4 ng/mL) was used as the positive control. One representative Western blot is shown. (−) means untreated control. (B) Effect of BHA on pJNK activation by MNP in Western blot analysis. BHA (200 μM) was added 30 min prior to particle stimulation. One representative Western blot is shown.

MNP (200 μg/cm^2) diminished and delayed the degree of IκBα degradation (Figure 13, (2)). Treatment with 1 mmol/L sodium arsenite completely prevented TNFα-mediated IκBα degradation and served as a positive control. To study whether the effect on IκBα degradation may be due to stress-induced Hsp70, as shown by Wong et al.,[48] Western blotting was performed. Unstimulated A549 cells already showed Hsp70 expression, which did not further increase upon treatment with MNP (data not shown).

Activation of JNK. A549 cells were treated with MNP (100 μg/cm^2) for 10 to 36 h. A combination of actinomycin D (333 nmol/L) and TNFα (4 ng/mL) was used as a positive control. MNP led to a strong and elongated activation of JNK after exposure times of 10 to 24 h (see Figure 14A). At shorter incubation times (1 to 6 h, data not shown) no p-JNK activation was observed. Interestingly, the particle treatment also led to a slight increase in total JNK compared to that of the negative control demonstrating a stress response of the cells. To determine whether JNK activation is due to ROS production, the ROS-scavenger BHA (200 μmol/L) was added 30 min before particle treatment (Figure 14B). Addition of BHA could not inhibit or decrease the formation of p-JNK, indicating a ROS-independent way of JNK activation. The same result was obtained with the ROS-scavenger NAC in concentrations of 1 to 2 mmol/L (data not shown).

DISCUSSION

Magnetite (Fe_3O_4) is an abundant component of ambient PM occurring in various sizes. Until now, several studies on biological effects of MNP exist,[11,21,22] but systematic studies on the possible cytotoxic and genotoxic effects as a function of grain size are still rare. To fill this gap, we have carried out uptake experiments as well as biological studies with magnetite fractions of defined sizes. Our TEM analyses of ultrathin sections provided clear evidence that bulk magnetite and MNP were incorporated into A549 human lung cells (Figures 3 and 4). The observed features indicate that the particles were taken up by phagocytosis and/or macropinocytosis (Figure 3C), as also described for other fine particles and nanoparticles.[49] Bulk magnetite and MNP were mainly found as aggregates in membrane-bound vesicles. The lack of MNP on the cell surface might indicate that, during the exposure time of 24 h, MNP are more rapidly taken up by A549 cells than the larger particles of the bulk fraction. However, it cannot be excluded that, in contrast to the MNP, the larger bulk magnetite particles have not been washed off during the washing and embedding processes. Therefore, further experiments are necessary.

These phagocytosed particles cause slight cytotoxic effects. As the sensitivity of the different assays can differ depending on the underlying mechanisms, which lead to loss of cell viability, two methods were used to study the cell viability. Cell cultures exposed to magnetite particles showed only a slight decrease in cell viability or none at all, as measured by the WST-1 assay (Figure 5), whereas the NR uptake did not show an increased cytotoxicity (Figure 6) but an increased NR-dye uptake. An increased NR uptake after exposure to various NPs or chemicals in a subcytotoxic concentration is also described by other authors.[37,50,51] This effect probably occurs due to enhanced lysosomal activity through particle uptake and lysosomal distension. In cell-based assays, the influence of FBS on iron oxide particles also needs to be considered. Particles might be coated by serum proteins and thus loose their surface reactivity, which would lead to a lower cytotoxicity.[52–55] To study the level of these interactions, the WST-1 assay was performed with different FBS concentrations. The reduced serum content did not significantly affect the results (data not shown).

Particles can damage the mitochondria, which results in decreased conversion of formazan, measured by the WST-1

assay or by the more sensitive mitochondrial membrane depolarization, an early apoptotic marker. In the current study, we observed an increase in mitochondrial membrane depolarization for MNP (Figure 8), whereas the WST-assay showed no decrease in cell viability (Figure 5). Disturbance of the mitochondrial membrane was found by Karlsson et al., who reported a significant increase in mitochondrial membrane depolarization for magnetite bulk particles at a concentration of 40 $\mu g/cm^2$.[28] Damage to the mitochondria can lead to ROS formation and trigger apoptosis, which did not occur under the conditions studied (data not shown). However, after the endocytosis of magnetite, we observed an increased concentration-dependent ROS formation in A549 cells, which was independent of the particle size (Figure 7). The mechanism of ROS production due to magnetite is still not clear. According to our results, it is most likely that ROS are being generated by interactions between magnetite and cellular components, such as the mitochondria. It is rather unlikely, that iron release through dissolution of magnetite is responsible for the observed effects. If iron is bioavailable in lung cells, it is known to be potentially toxic through Fenton- and Haber-Weiss-type reactions, which lead to increased ROS generation and cell death.[13,56] We observed no increased ROS formation after exposure to the supernatant preincubated for 24 h with bulk or MNP; moreover, other studies have also demonstrated that the capability of magnetite particles to release free radicals is marginal due to their low surface reactivity.[57,58] Since the observed cytotoxic effect is very low, we assume that only small amounts of iron ions are released by magnetite and that consequently only small amounts of ROS are produced, which might be inactivated by the radical-scavenging enzymes in A549 cells.[59] Another possible mechanism is the phagocytosis-related formation of ROS. Uptake of particles via phagocytosis can lead to an activation of the membrane-bound NADPH oxidase, which catalyzes the conversion of oxygen to superoxide radicals.[60]

We also demonstrated that magnetite particles are able to cause stable chromosomal damage in a concentration-dependent manner. Fractions containing the smaller particles induced the highest formation of micronuclei (Bulk, AF, MNP), whereas RF showed lower activity (Figure 10). The bulk fraction covers all of the size fractions tested but mainly those with a size smaller than 1.6 μm. Genotoxic effects were confirmed by the Comet assay, in which the bulk fraction and MNP showed the highest DNA damage (Figure 9). These results are consistent with Karlsson et al., who found DNA-damaging effects for bulk magnetite (average size <1 μm) and MNP (20−30 nm) in A549 cells.[28] Additionally, we could show that larger particles with a mean diameter of 2.5 μm (RF) induced less pronounced DNA damage, indicating that this size fraction may be less harmful to A549 cells.

Only one magnetite nanoparticle has been found in about 100 screened nuclei. Most of the particles were incorporated into cytoplasmic vesicles (Figure 4). Therefore, the observed genotoxic effects are presumably not due to direct particle−DNA interaction in the nucleus of A549 cells. However, another mechanism of primary direct genotoxicity caused by particulates, especially UFP, has been suggested by Gonzales et al.[61] The authors assume that mechanical interferences between UFP and components of the cytoskeleton during cell division may play a role. Our data document attenuation of the DNA and chromosomal damages by the ROS-scavengers NAC and BHA (Figure 11) and thus indicate that ROS were involved in the observed genotoxic effects of magnetite. Karlsson et al. have also observed significant oxidative DNA damage when A549 cells were exposed for 4 h to 40 $\mu g/cm^2$ of MNP (20−30 nm) and bulk magnetite (average size < 1 μm).[28] As discussed above, an oxidative attack of the DNA through free radical release of magnetite is unlikely, due to its low surface reactivity.[58] We conclude that the indirect primary genotoxicity, the enhanced production of ROS caused by mitochondria or membrane-bound NADPH oxidases in response to their interaction with magnetite, might be a possible mechanism.[52] An increased ROS production may weaken the antioxidant defense through depletion of intracellular antioxidants (e.g., glutathione), resulting in oxidative stress and increased DNA damage. Not yet clearly demonstrated for particulates, Beyersmann and Hartwig observed that inactivation of specific DNA repair proteins by various metal ions can lead to genotoxic effects.[62]

Since endogenous ROS are known to either activate or inhibit the transcription factor NF-κB depending on concentration,[63] we studied the effects of bulk magnetite and MNP on NF-κB-DNA activation in A549 cells by using EMSA at different concentrations and durations. NF-κB is a pivotal mediator, which is involved in multiple cellular responses to a variety of stimuli, including cytokines and ROS, and which regulates the transcription of various pro- and inflammatory mediators.[63−65] However, no activating effect on NF-κB was observed by MNP or bulk (Figure 12A), but a slight decrease in NF-κB when cells were additionally treated with TNFα was observed. The same results were obtained by Shen et al. in HeLa cells, who found neither an enhanced NF-κB activity nor an upregulation of NF-κB regulated target genes.[26] It can be speculated that either ROS are deactivated by intracellular enzymes or that the ROS formation may have a negative impact on NF-κB activity in A549 cells.[63]

As the JNK cascade is also mediated by ROS,[63] we investigated the effect of MNP on JNK activation. Interestingly, incubation with MNP led to a sustained activation of JNK (Figure 14A), but activation was not abolished by the ROS scavengers BHA or NAC (Figure 14B). Hence, it could be concluded that JNK activation does not seem to be ROS-dependent. Since it is well known that sustained JNK activation can trigger apoptosis,[66] we expected increased apoptosis. We observed only slight cytotoxic effects after the exposure of magnetite bulk particles to A549 cells, which may be explained by the observed decrease of the mitochondrial membrane potential after exposure to bulk magnetite and MNP. Nevertheless, neither the mitochondrial depolarization and associated ROS release nor the DNA damage was sufficient to induce cell death. Moreover, the other fractions did not show any increased cytotoxicity. Further studies have to clarify the role of ROS in the interplay among NF-κB, JNK activation, and cell survival.

Furthermore, pretreatment with MNP and poststimulation with TNFα, simulating an acute inflammation, decreased TNFα-induced NF-κB DNA binding (Figure 12B). In addition we could also demonstrate a diminished and delayed TNFα-induced degradation of IκBα after treatment with MNP (Figure 13). Similar effects were described by Wong et al. when A549 cells were pretreated with sodium arsenite under the same conditions, but here, IκBα degradation was inhibited to a much higher degree.[48] These authors were able to provide evidence that sodium arsenite decreased TNFα-mediated NF-κB nuclear translocation by stabilization and increased expression of IκB due to the induction of stress response, in this case by expression of Hsp70. Furthermore, Kawata et al. observed a particle induced

upregulation of Hsp70 for Ag-NP in HepG2 cells.[67] In contrast to these results, we found Hsp70 already highly upregulated in untreated A549 cells suggesting a Hsp70-independent mechanism of the diminished degradation of IκBα after treatment with MNP. However, we also need to consider that the effect on IκBα degradation was only moderate in our studies, and hence, the effect on Hsp70 may be too low to be detected. Jaatela et al. observed that Hsp70 did not inhibit activation of JNK or caspase 3 activity but without leading to apoptosis.[68] Taken together, high amounts of Hsp70 are constitutively expressed in untreated A549 cells, suggesting a high upregulation of the protective system against acute lung injury. This results in a rescue of A549 cells from apoptosis even after MMP decrease and ROS formation caused by exposure to different concentrations of magnetite occurs.

In summary, exposure of A549 cells to different size fractions of magnetite particles enhanced ROS production to a significant extent after 24 h. This effect was accompanied by only slight cytotoxicity and an increased mitochondrial membrane depolarization. Furthermore, our study clearly demonstrates that magnetite particles induce concentration-dependent DNA damage, as revealed by the Comet assay and the CB-MNvit. A slight size dependency could be observed, as the larger particles induced less genotoxicity. These effects were partially blocked by addition of the ROS scavengers NAC (1 mmol/L) or BHA (100 μmol/L), indicating that ROS play an important role in magnetite-induced genotoxicity. Our results show that only the MNP have properties affecting signaling pathways and are able to trigger immunological effects. MNP induced activation of JNK but not NF-κB and this activation was ROS-independent. Nevertheless, a mutual interaction cannot be ruled out between ROS, JNK, and NF-κB, and this should be the focus of further studies. The concentrations of particles used in the present study seem to be high compared with that in human exposure conditions. However, it is likely that after inhalation magnetite would be deposited for a long time in the respiratory tract and other tissues.

The observed *in vitro* reactivity of magnetite gives rise to concern due to the high number of people that are exposed occupationally and environmentally to iron oxide-containing PM. To what extent magnetite particles cause health effects in humans needs to be further evaluated. Therefore, additional studies should be performed to investigate the long-term risk of magnetite-induced chronic effects.

AUTHOR INFORMATION

Corresponding Author

*Department of Environmental Health Sciences, University Medical Center Freiburg, Breisacher Str. 115b, D-79106 Freiburg, Germany. E-mail: mathias.koenczoel@uniklinik-freiburg.de.

ACKNOWLEDGMENT

We thank Andrea Stokes, Beat Haenni, and Mohammed Ouanella from the Institute of Anatomy in Bern, Switzerland for TEM-sample preparation and Robert Burzan from the Department of Environmental Health Science in Freiburg for Comet assay slide preparation. We express our special gratitude to Sigrid Hirth-Walther, Angela Thiemann, and Isolde Schmidt for performing the AAS, laser-diffraction, and XRD analyses in the laboratories of the Institute of Geosciences at the University of Freiburg. We thank Alexander Burkhardt for providing assistance with the PCS measurement.

REFERENCES

(1) Brook, R. D., Rajagopalan, S., Pope, C. A., Brook, J. R., Bhatnagar, A., ez-Roux, A. V., Holguin, F., Hong, Y. L., Luepker, R. V., Mittleman, M. A., Peters, A., Siscovick, D., Smith, S. C., Whitsel, L., and Kaufman, J. D. (2010) Particulate matter air pollution and cardiovascular disease. An update to the scientific statement from the American Heart Association. *Circulation 121* (21), 2331–2378.

(2) WHO (2004) Health aspects of air pollution. Results from the WHO project "Systematic review of health aspects of air pollution in Europe, Kopenhagen, Denmark.

(3) Pelucchi, C., Negri, E., Gallus, S., Boffetta, P., Tramacere, I., and La Vecchia, C. (2009) Long-term particulate matter exposure and mortality: a review of European epidemiological studies. *BMC Public Health 9*, 453.

(4) Pope, C. A., Burnett, R. T., Thun, M. J., Calle, E. E., Krewski, D., Ito, K., and Thurston, G. D. (2002) Lung cancer, cardiopulmonary mortality, and long-term exposure to fine particulate air pollution. *J. Am. Med. Assoc. 287* (9), 1132–1141.

(5) Nel, A., Xia, T., Madler, L., and Li, N. (2006) Toxic potential of materials at the nanolevel. *Science 311* (5761), 622–627.

(6) Gieré, R., and Querol, X. (2010) Solid Particulate Matter in the Atmosphere. *Elements 6* (4), 215–222.

(7) Grobéty, B., Gieré, R., Dietze, V., and Stille, P. (2010) Airborne particles in the urban environment. *Elements 6* (4), 229–234.

(8) Oberdorster, G., Oberdorster, E., and Oberdorster, J. (2005) Nanotoxicology: An emerging discipline evolving from studies of ultrafine particles. *Environ. Health Perspect. 113* (7), 823–839.

(9) Peters, A., Wichmann, H. E., Tuch, T., Heinrich, J., and Heyder, J. (1997) Respiratory effects are associated with the number of ultrafine particles. *Am. J. Respir. Crit. Care Med. 155* (4), 1376–1383.

(10) Schulz, H., Harder, V., Ibald-Mulli, A., Khandoga, A., Koenig, W., Krombach, F., Radykewicz, R., Stampfl, A., Thorand, B., and Peters, A. (2005) Cardiovascular effects of fine and ultrafine particles. *J. Aerosol Med. 18* (1), 1–22.

(11) Lewinski, N., Colvin, V., and Drezek, R. (2008) Cytotoxicity of nanoparticles. *Small 4* (1), 26–49.

(12) Donaldson, K., Tran, L., Jimenez, L. A., Duffin, R., Newby, D. E., Mills, N., MacNee, W., and Stone, V. (2005) Combustion-derived nanoparticles: a review of their toxicology following inhalation exposure. *Part. Fibre Toxicol. 2*, 10.

(13) Upadhyay, D., Panduri, V., Ghio, A., and Kamp, D. W. (2003) Particulate matter induces alveolar epithelial cell DNA damage and apoptosis: Role of free radicals and the mitochondria. *Am. J. Respir. Cell Mol. Biol. 29* (2), 180–187.

(14) Schins, R. P. F., and Knaapen, A. M. (2007) Genotoxicity of poorly soluble particles. *Inhalation Toxicol. 19*, 189–198.

(15) Ball, B. R., Smith, K. R., Veranth, J. M., and Aust, A. E. (2000) Bioavailability of iron from coal fly ash: Mechanisms of mobilization and of biological effects. *Inhalation Toxicol. 12*, 209–225.

(16) Gminski, R., Decker, K., Heinz, C., Seidel, A., Könczöl, M., Goldenberg, E., Grobéty, B., Ebner, W., Gieré, R., and Mersch-Sundermann, V. (2011) Genotoxic effects of three selected black toner powders and their dimethyl sulfoxide extracts in cultured human epithelial A549 lung cells in vitro. *Environ. Mol. Mutagen. 52* (4), 296–309.

(17) Johansson, C., and Johansson, P. A. (2003) Particulate matter in the underground of Stockholm. *Atmos. Environ. 37* (1), 3–9.

(18) Murruni, L. G., Solanes, V., Debray, M., Kreiner, A. J., Davidson, J., Davidson, M., Vazquez, M., and Ozafran, M. (2009) Concentrations and elemental composition of particulate matter in the Buenos Aires underground system. *Atmos. Environ. 43* (30), 4577–4583.

(19) Lorenzo, R., Kaegi, R., Gehrig, R., and Grobety, B. (2006) Particle emissions of a railway line determined by detailed single particle analysis. *Atmos. Environ. 40* (40), 7831–7841.

(20) Sowards, J. W., Lippold, J. C., Dickinson, D. W., and Ramirez, A. J. (2008) Characterization of welding fume from SMAW electrodes. Part I. *Weld. J. 87* (4), 106–112.

(21) Figuerola, A., Di, C. R., Manna, L., and Pellegrino, T. (2010) From iron oxide nanoparticles towards advanced iron-based inorganic

materials designed for biomedical applications. *Pharmacol. Res. 62* (2), 126–143.

(22) Duguet, E., Vasseur, S., Mornet, S., and Devoisselle, J. M. (2006) Magnetic nanoparticles and their applications in medicine. *Nanomedicine 1* (2), 157–168.

(23) Berry, C. C., Wells, S., Charles, S., Aitchison, G., and Curtis, A. S. (2004) Cell response to dextran-derivatised iron oxide nanoparticles post internalisation. *Biomaterials 25* (23), 5405–5413.

(24) Zhang, Y., Kohler, N., and Zhang, M. (2002) Surface modification of superparamagnetic magnetite nanoparticles and their intracellular uptake. *Biomaterials 23* (7), 1553–1561.

(25) Cheng, F. Y., Su, C. H., Yang, Y. S., Yeh, C. S., Tsai, C. Y., Wu, C. L., Wu, M. T., and Shieh, D. B. (2005) Characterization of aqueous dispersions of Fe3O4 nanoparticles and their biomedical applications. *Biomaterials 26* (7), 729–738.

(26) Shen, S. S., Uu, Y. X., Huang, P. L., and Wang, J. K. (2009) In vitro cellular uptake and effects of Fe_3O_4magnetic nanoparticles on HeLa cells. *J. Nanosci. Nanotechnol. 9* (5), 2866–2871.

(27) Karlsson, H. L., Cronholm, P., Gustafsson, J., and Moller, L. (2008) Copper oxide nanoparticles are highly toxic: a comparison between metal oxide nanoparticles and carbon nanotubes. *Chem. Res. Toxicol. 21* (9), 1726–1732.

(28) Karlsson, H. L., Gustafsson, J., Cronholm, P., and Moller, L. (2009) Size-dependent toxicity of metal oxide particles: A comparison between nano- and micrometer size. *Toxicol. Lett. 188* (2), 112–118.

(29) Ankamwar, B., Lai, T. C., Huang, J. H., Liu, R. S., Hsiao, M., Chen, C. H., and Hwu, Y. K. (2010) Biocompatibility of Fe_3O_4 nanoparticles evaluated by in vitro cytotoxicity assays using normal, glia and breast cancer cells. *Nanotechnology 21* (7), 75102.

(30) Auffan, M. ü., Achouak, W., Rose, J. ü. m., Roncato, M. A., Chanéac, C., Waite, D. T., Masion, A., Woicik, J. C., Wiesner, M. R., and Bottero, J. Y. (2008) Relation between the redox state of iron-based nanoparticles and their cytotoxicity toward *Escherichia coli*. *Environ. Sci. Technol. 42* (17), 6730–6735.

(31) Hussain, S. M., Hess, K. L., Gearhart, J. M., Geiss, K. T., and Schlager, J. J. (2005) In vitro toxicity of nanoparticles in BRL 3A rat liver cells. *Toxicol. in Vitro 19* (7), 975–983.

(32) Pickard, M. R., and Chari, D. M. (2010) Robust uptake of magnetic nanoparticles (MNPs) by central nervous system (CNS) microglia: Implications for particle uptake in mixed neural cell populations. *Int. J. Mol. Sci. 11* (3), 967–981.

(33) Zhu, M. T., Yun, W., Feng, W. Y., Bing, W., Meng, W., Hong, O. Y., and Chai, Z. F. (2010) Oxidative stress and apoptosis induced by iron oxide nanoparticles in cultured human umbilical endothelial cells. *J. Nanosci. Nanotechnol. 10* (12), 8584–8590.

(34) Park, E. J., Kim, H., Kim, Y., Yi, J., Choi, K., and Park, K. (2010) Inflammatory responses may be induced by a single intratracheal instillation of iron nanoparticles in mice. *Toxicology 275* (1−3), 65–71.

(35) Lieber, M., Smith, B., Szakal, A., Nelson-Rees, W., and Todaro, G. (1976) A continuous tumor-cell line from a human lung carcinoma with properties of type II alveolar epithelial cells. *Int. J. Cancer 17* (1), 62–70.

(36) Muhlfeld, C., Rothen-Rutishauser, B., Vanhecke, D., Blank, F., Gehr, P., and Ochs, M. (2007) Visualization and quantitative analysis of nanoparticles in the respiratory tract by transmission electron microscopy. *Part. Fibre Toxicol. 4*, 11.

(37) Repetto, G., del, P. A., and Zurita, J. L. (2008) Neutral red uptake assay for the estimation of cell viability/cytotoxicity. *Nat. Protoc. 3* (7), 1125–1131.

(38) Olson, B. J., and Markwell, J. (2007) Assays for determination of protein concentration. *Curr. Protoc. Protein Sci.*, Chapter 3, Unit 3.4

(39) Zhao, Y., Yang, G., Ren, D., Zhang, X., Yin, Q., and Sun, X. (2011) Luteolin suppresses growth and migration of human lung cancer cells. *Mol. Biol. Rep. 38* (2), 1115–1119.

(40) Singh, N. P., Mccoy, M. T., Tice, R. R., and Schneider, E. L. (1988) A simple technique for quantitation of low-levels of dna damage in individual cells. *Exp. Cell Res. 185* (2), 184–191.

(41) Tice, R. R., Agurell, E., Anderson, D., Burlinson, B., Hartmann, A., Kobayashi, H., Miyamae, Y., Rojas, E., Ryu, J. C., and Sasaki, Y. F. (2000) Single cell gel/comet assay: Guidelines for in vitro and in vivo genetic toxicology testing. *Environ. Mol. Mutagen. 35* (3), 206–221.

(42) OECD (2010) Test No. 487: In Vitro Mammalian Cell Micronucleus Test (MNvit), OECD Guidelines for Testing of Chemicals, OECD, Paris, France.

(43) Fenech, M. (2000) The in vitro micronucleus technique. *Mutat. Res., Fundam. Mol. Mech. Mutagen. 455* (1−2), 81–95.

(44) Fenech, M. (2007) Cytokinesis-block micronucleus cytome assay. *Nat. Protoc. 2* (5), 1084–1104.

(45) Umegaki, K., and Fenech, M. (2000) Cytokinesis-block micronucleus assay in WIL2-NS cells: a sensitive system to detect chromosomal damage induced by reactive oxygen species and activated human neutrophils. *Mutagenesis 15* (3), 261–269.

(46) Surralles, J., Xamena, N., Creus, A., Catalan, J., Norppa, H., and Marcos, R. (1995) Induction of micronuclei by 5 pyrethroid insecticides in whole-blood and isolated human lymphocyte-cultures. *Mutat. Res., Genet. Toxicol. 341* (3), 169–184.

(47) Schreiber, E., Matthias, P., Muller, M. M., and Schaffner, W. (1989) Rapid detection of octamer binding-proteins with mini-extracts, prepared from a small number of cells. *Nucleic Acids Res. 17* (15), 6419.

(48) Wong, H. R., Ryan, M., and Wispe, J. R. (1997) Stress response decreases NF-kappa B nuclear translocation and increases I-kappa B alpha expression in A549 cells. *J. Clin. Invest. 99* (10), 2423–2428.

(49) Rothen-Rutishauser, B., Blank, F., Mühlfeld, C.-H., and Gehr, P. (2009) Nanoparticle-Cell Membrane Interactions, in *Particle-Lung Interactions* (Gehr, P., Blank, F., Mühlfeld, C.-H., and Rothen-Rutishauser, B., Eds.) Informa Healthcare, New York.

(50) Lanone, S., Rogerieux, F., Geys, J., Dupont, A., Maillot-Marechal, E., Boczkowski, J., Lacroix, G., and Hoet, P. (2009) Comparative toxicity of 24 manufactured nanoparticles in human alveolar epithelial and macrophage cell lines. *Part. Fibre Toxicol. 6* (1), 14.

(51) Weyermann, J., Lochmann, D., and Zimmer, A. (2005) A practical note on the use of cytotoxicity assays. *Int. J. Pharm. 288* (2), 369–376.

(52) Donaldson, K., Poland, C. A., and Schins, R. P. F. (2010) Possible genotoxic mechanisms of nanoparticles: Criteria for improved test strategies. *Nanotoxicology 4* (4), 414–420.

(53) Geys, J., Nemery, B., and Hoet, P. H. M. (2010) Assay conditions can influence the outcome of cytotoxicity tests of nanomaterials: Better assay characterization is needed to compare studies. *Toxicol. in Vitro 24* (2), 620–629.

(54) Okeson, C. D., Riley, M. R., and Riley-Saxton, E. (2004) In vitro alveolar cytotoxicity of soluble components of airborne particulate matter: effects of serum on toxicity of transition metals. *Toxicol. in Vitro 18* (5), 673–680.

(55) Schulze, C., Kroll, A., Lehr, C. M., Schäfer, U. F., Becker, K., Schnekenburger, J., Schulze Isfort, C., Landsiedel, R., and Wohlleben, W. (2008) Not ready to use - overcoming pitfalls when dispersing nanoparticles in physiological media. *Nanotoxicology 2* (2), 51–61.

(56) Nunez, M. T., Garate, M. A., Arredondo, M., Tapia, V., and Munoz, P. (2000) The cellular mechanisms of body iron homeostasis. *Biol. Res. 33* (2), 133–142.

(57) Berger, M., Dehazen, M., Nejjari, A., Fournier, J., Guignard, J., Pezerat, H., and Cadet, J. (1993) Radical oxidation reactions of the purine moiety of 2′-deoxyribonucleosides and Dna by iron-containing minerals. *Carcinogenesis 14* (1), 41–46.

(58) Fubini, B., and Mollo, L. (1995) Role of iron in the reactivity of mineral fibers. *Toxicol. Lett. 82−3*, 951–960.

(59) Limbach, L. K., Wick, P., Manser, P., Grass, R. N., Bruinink, A., and Stark, W. J. (2007) Exposure of engineered nanoparticles to human lung epithelial cells: Influence of chemical composition and catalytic activity on oxidative stress. *Environ. Sci. Technol. 41* (11), 4158–4163.

(60) Nabeshi, H., Yoshikawa, T., Matsuyama, K., Nakazato, Y., Tochigi, S., Kondoh, S., Hirai, T., Akase, T., Nagano, K., Abe, Y., Yoshioka, Y., Kamada, H., Itoh, N., Tsunoda, S. i., and Tsutsumi, Y. (2011) Amorphous nanosilica induce endocytosis-dependent ROS generation and DNA damage in human keratinocytes. *Part. Fibre Toxicol. 8* (1), 1.

(61) Gonzalez, L., Thomassen, L. C. J., Plas, G., Rabolli, V., Napierska, D., Decordier, I., Roelants, M., Hoet, P. H., Kirschhock, C. E. A., Martens, J. A., Lison, D., and Kirsch-Volders, M. (2010) Exploring the aneugenic and clastogenic potential in the nanosize range: A549 human lung carcinoma cells and amorphous monodisperse silica nanoparticles as models. *Nanotoxicology 4* (4), 382–395.

(62) Beyersmann, D., and Hartwig, A. (2008) Carcinogenic metal compounds: recent insight into molecular and cellular mechanisms. *Arch. Toxicol. 82* (8), 493–512.

(63) Bubici, C., Papa, S., Dean, K., and Franzoso, G. (2006) Mutual cross-talk between reactive oxygen species and nuclear factor-kappa B: molecular basis and biological significance. *Oncogene 25* (51), 6731–6748.

(64) Bonizzi, G., and Karin, M. (2004) The two NF-kappa B activation pathways and their role in innate and adaptive immunity. *Trends Immunol. 25* (6), 280–288.

(65) Vallabhapurapu, S., and Karin, M. (2009) Regulation and function of NF-kappa B transcription factors in the immune system. *Annu. Rev. Immunol. 27*, 693–733.

(66) Chen, Y. R., and Tan, T. H. (2000) The c-Jun N-terminal kinase pathway and apoptotic signaling. *Int. J. Oncol. 16* (4), 651–662.

(67) Kawata, K., Osawa, M., and Okabe, S. (2009) In vitro toxicity of silver nanoparticles at noncytotoxic doses to HepG2 human hepatoma cells. *Environ. Sci. Technol. 43* (15), 6046–6051.

(68) Jaattela, M., Wissing, D., Kokholm, K., Kallunki, T., and Egeblad, M. (1998) Hsp70 exerts its anti-apoptotic function downstream of caspase-3-like proteases. *EMBO J. 17* (21), 6124–6134.